JPET Fast Forward. Published on November 8, 2012 as DOI: 10.1124/jpet.112.198697

JPET 198697

Using Chimeric Mice with Humanized Livers to Predict Human Drug Metabolism and a Drug-Drug Interaction[a]

Toshihiko Nishimura*, Yajing Hu*, Manhong Wu, Edward Pham, Hiroshi Suemizu, Menashe Elazar, Michael Liu, Ramazan Idilman, Cihan Yurdaydin, Peter Angus, Catherine Stedman, Brian Murphy, Jeffrey Glenn, Masato Nakamura, Tatsuji Nomura, Yuan Chen, Ming Zheng, William L. Fitch, and Gary Peltz[#]

From the Department of Anesthesia Stanford University School of Medicine, Stanford CA 94305 (TN, YH, MW, MZ, WLF, GP); The Department of Medicine, Stanford University School of Medicine, Stanford CA 94305 (EP, ME, ML, JG); Central Institute for Experimental Animals, 3-25-12 Tonomachi, Kawasaki-ku, Kawasaki, Kanagawa 210-0821, Japan (HS, MN, TN); and Genentech, Drug Metabolism and Pharmacokinetics, 1 DNA Way, South San Francisco, CA 94080, United States (YN); Hepatology Institute, University of Ankara, Turkey 06100 (RI, CY); Liver Transplant Unit, University of Melbourne, Austin Hospital, Heidelberg 3084, Australia (PA); Gastroenterology Department, Christchurch Hospital, and University of Otago, Christchurch, New Zealand (CS) ; Eiger BioPharmaceuticals, Palo Alto CA 94303 (BM).

JPET198697

Running Title: Chimeric Mice and Human Drug Metabolism

#Address correspondence to: gpeltz@stanford.edu, 300 Pasteur Dr, Stanford, CA 94305, phone: 650 721 2487.

This manuscript contains:

37 references
4 Figures
2 tables
The text of the paper is contained on pages 4 to 16 of this submission
The number of words:

Abstract	180
Introduction	638
Discussion	749

Recommended Section Assignment: Drug Discovery and Translational Medicine

Abbreviations: AUC, area under the concentration-time curve; CYP450, cytochrome P450; DDI, drug-drug interaction; ESI, electrospray ionization; FAH, fumarylacetoacetate hydrolase; GCV, ganciclovir; LC/MS, liquid chromatography coupled with mass spectroscopy; MS/MS, tandem mass spectroscopy; TK-NOG, NOG mouse expressing a thymidine kinase transgene;

Abstract

Inter-species differences in drug metabolism have made it difficult to use pre-clinical animal testing data to predict the drug metabolites or potential drug-drug interactions (**DDI**) that will occur in humans. Although chimeric mice with humanized livers can produce known human metabolites for test substrates, we do not know whether chimeric mice can be used to prospectively predict human drug metabolism or a possible DDI. Therefore, we investigated whether they could provide a more predictive assessment for clemizole, a drug in clinical development for the treatment of hepatitis C virus (**HCV**) infection. Our results demonstrate, for the first time, that analyses performed in chimeric mice can correctly identify the predominant human drug metabolite prior to human testing. The differences in the rodent and human pathways for clemizole metabolism were of importance, since the predominant human metabolite was found to have synergistic anti-HCV activity. Moreover, studies in chimeric mice also correctly predicted that a DDI would occur in humans when clemizole was co-administered with a CYP3A4 inhibitor. These results demonstrate that using chimeric mice can improve the quality of pre-clinical drug assessment.

JPET Fast Forward. Published on November 8, 2012 as DOI: 10.1124/jpet.112.198697
This article has not been copyedited and formatted. The final version may differ from this version.

Introduction

Existing *in vitro* systems and *in vivo* testing in animal species have not always accurately predicted human pharmacokinetics or the human-specific drug metabolism pathways for candidate medications (Anderson et al., 2009; Leclercq et al., 2009; Walker et al., 2009). Inter-species differences in drug metabolism produce qualitative and quantitative differences between the drug metabolites produced in humans and animal species. The inability to pre-clinically identify the human-specific drug metabolites is particularly problematic; since it is most often a drug metabolite, and not the parent drug itself, that is responsible for an unexpected drug-induced toxicity (Guengerich and MacDonald, 2007; Smith and Obach, 2009). If a candidate drug has a human-specific (or more often, a human-predominant) drug metabolite, the utility of preclinical toxicity testing in animal species is quite limited (Anderson et al., 2009; Leclercq et al., 2009).

To address this problem, we (Hasegawa et al., 2011) and others (reviewed in (Yoshizato and Tateno, 2009; de Jong et al., 2010)) have developed chimeric mice, in which mouse liver is replaced by transplanted human liver cells or tissue-engineered human liver (Chen et al., 2011). In one model system, uroplasminogen activator transgene expression facilitates the growth of transplanted human liver cells (Vyse et al., 1980; Tateno et al., 2004; Meuleman et al., 2005; Azuma et al., 2007; Katoh and Yokoi, 2007); while a fumarylacetoacetate hydrolase (*Fah*) knockout mouse is used in the other system (Azuma et al., 2007) (Bissig et al., 2010). We recently produced a new model system for human liver replacement. In this new system, a herpes simplex virus type 1 thymidine kinase (**TK**) transgene was expressed within the liver of a highly immunodeficient mouse strain (**NOG**) (Ito et al., 2002) to produce the **TK-NOG** transgenic mouse (Hasegawa et al., 2011). A brief exposure to a non-toxic dose of ganciclovir (**GCV**) causes a rapid and temporally controlled ablation of mouse liver cells expressing the transgene,

which enabled the transplanted human liver cells to develop into a mature “human organ” with a 3-dimensional architecture and gene expression pattern (including many human drug metabolizing enzymes and transporters) characteristic of mature human liver. The absence of ongoing liver toxicity in the TK-NOG mice enabled the humanized liver to be stably maintained for >8 months without exogenous drug treatments. The humanized liver in chimeric TK-NOG mice was shown to express mRNAs encoding human CYP450 enzymes, transporters and transcription factors affecting drug metabolism at levels that were equivalent to those in the donor human hepatocytes. Moreover, there was extensive human CYP3A4 protein expression in the humanized livers, and chimeric TK-NOG mice could mediate human-specific drug biotransformation reactions (Hasegawa et al., 2011).

There are multiple examples where chimeric mice have been shown to produce known human-specific metabolites for several test substrates (Chen et al., 2011) (Hasegawa et al., 2011) (Tateno et al., 2004) (Katoh and Yokoi, 2007), including steroids (Katoh et al., 2007) (Lootens et al., 2009) (Pozo et al., 2009) (Kamimura et al., 2010). However, we do not know if chimeric mice can be used to predict the pattern of human drug metabolism for a candidate therapeutic prior to human clinical testing. In one recent study, chimeric mice produced mixed results when their ability to predict the pattern of human drug metabolism was assessed (De Serres et al., 2011). We also do not know if chimeric mice can be used to prospectively evaluate the potential for a DDI involving a candidate therapeutic to occur in human subjects. Since more than 30% of the US population over 57 years of age take 5 or more prescription drugs at a given time, DDIs have created major problems for patients, and for regulatory authorities (Zhang et al., 2010). However, using available *in vitro* or *in vivo* animal models, it has been difficult to predict many of the clinically important DDIs, which only became apparent after drug development was completed (Bode, 2010). Therefore, we investigated whether TK-NOG mice with ‘humanized livers’ could provide more predictive information about the human metabolic pathways and

JPET Fast Forward. Published on November 8, 2012 as DOI: 10.1124/jpet.112.198697
This article has not been copyedited and formatted. The final version may differ from this version.

metabolites for a candidate therapeutic, which is being developed as a novel treatment for HCV infection. Clemizole, an antihistamine drug that was once widely used for treatment of allergic disease, was recently discovered to be a potent inhibitor (IC50 24 nM) of the interaction between a HCV protein (NS4B) and HCV RNA (Einav et al., 2008). Although clemizole was widely utilized in the 1950's and 1960's, this was before contemporary regulatory requirements were established for new drug development, and we have very minimal information about its pharmacokinetics and metabolism.

Methods

Chemicals and reagents. For *in vitro* and animal experiments, clemizole hydrochloride and omeprazole were purchased from Sigma (St. Louis, MO); ritonavir was purchased from Santa Cruz Biotechnology (Santa Cruz, CA). Pooled Human liver microsomes, male rat and mouse liver microsomes were purchased from BD Gentest (Woburn,MA). Cryopreserved human hepatocytes and recombinant CYP450 enzymes were purchased from BD Biosciences (San Jose, CA, USA). Rat hepatocytes were freshly isolated according to standard procedures. All other chemicals were purchased from commercial sources and were of the highest purity available. Boceprevir was a gift from Leslie Holsinger (Virobay).

Mouse pharmacokinetic studies. All animal experiments were performed using protocols approved by the Stanford Institutional Animal Care and Use Committee. Male C57BL6/J and Balb/c mice (8 weeks of age) were obtained from Jackson Labs and housed for 2 weeks prior to experimentation. NOG mice were obtained from In Vivo Sciences International (Sunnyvale, CA). Chimeric TK-NOG mice with humanized livers were prepared as described (Hasegawa et al., 2011), except the GCV dose was increased to 25 mg/kg, which was administered 7 and 5 days prior to human liver cell transplantation. The human albumin levels were determined using

JPET Fast Forward. Published on November 8, 2012 as DOI: 10.1124/jpet.112.198697
This article has not been copyedited and formatted. The final version may differ from this version.

previously described methods, and the human albumin concentration was shown to correlate with the extent of liver humanization (Hasegawa et al., 2011). The pharmacokinetic studies using these mice were performed 8-12 weeks after transplantation of human liver cells. Eight control NOG mice and eight humanized TK-NOG mice were administered 25 mg/kg clemizole PO, and blood samples were collected 30 minutes after dosing. The C57BL/6J mice (3 per time point) were dosed with 25 mg/kg PO Clemizole, and blood samples were collected at 15, 30 min and 1, 2, 4 and 6 hrs after dosing for analysis. For the DDI studies, eight humanized TK-NOG mice were dosed with Clemizole (25 mg/kg P.O.) with or without ritonavir (20 mg/kg P.O), and blood samples were collected 30 minutes after dosing. Six of these mice were also treated with debrisoquine (10 mg/kg PO), in the presence or absence of ritonavir (20 mg/kg PO), and plasma obtained 2 hr later for analysis.

Quantitative analysis of clemizole and metabolites in plasma. Mouse plasma (50 uL) was treated with acetonitrile with 0.1% formic acid (200 uL), vortexed and incubated at -20 ^{0}C for one hour, centrifuged at 10,000 rpm for 10 min. The supernatants were collected, dried and re-suspended in 50uL 5% acetonitrile with 0.1% formic acid for the analysis by LC/MS. HPLC was performed using an Agilent 1200 column compartment, capillary pump, and an autosampler on a Zorbax C18 column, 0.5x150 mm. The flow rate was 20 mL/min with a gradient from 5% solvent B (acetonitrile with 0.1% formic acid; solvent A is 0.1% formic acid in water) to 95% B in 30 min and held at 95% B for 5 min. Mass spectrometric analysis were carried out on an Agilent Model 6520 qTOF mass spectrometer equipped with an ESI source. The heated capillary temperature in the source was held at 325^{o}C. Full scan (m/z 110–1000) spectra or data dependent MS/MS spectra were collected. The metabolites were identified based on their collision-induced dissociation behavior in tandem mass spectrometry, accurate mass and retention time. Quantitative analysis of clemizole was performed using a calibration curve at 9-1257 ng/ml clemizole spiked into blank mouse plasma and extracted as above. An internal

JPET Fast Forward. Published on November 8, 2012 as DOI: 10.1124/jpet.112.198697
This article has not been copyedited and formatted. The final version may differ from this version.

standard 1-(p-bromobenzyl)-2-(1-pyrrolidinylmethyl)- Benzimidazole was also spiked in at 1000ng/ml. Relative amounts of clemizole and metabolites in each sample were calculated using the assumption that all compounds had the same MS response factor.

Statistical analysis. To assess the statistical significance of the differences in the relative amount of clemizole and its metabolites (M1, M2, M6, M12, M14 and M15) measured in plasma obtained from control and humanized TK-NOG mice (Table 1), or between control and ritonavir treated mice, a two-sample two-sided t test was used.

Human pharmacokinetic and metabolite studies. Phase 1b studies (to be reported elsewhere) were conducted in genotypes 1 and 2 HCV patients under IRB-approved protocols to investigate the safety and tolerability, pharmacokinetics, and pharmacodynamics of clemizole HCl (see www.Clinicaltrials.gov and approval by the University of Ankara Medical School Ethics Committee; study sponsor Eiger BioPharmaceuticals, Inc.). De-identified aliquots of excess material, which were not needed for clinical monitoring, were kindly provided by Wenjin Yang (Eiger BioPharmaceuticals, Inc.) to us for PK and metabolite analysis. The samples obtained were from human subjects that were administered 100 mg Clemizole P.O., with or without 100 mg ritonavir P.O. administered one hour before the clemizole, and blood samples were obtained 0 to 12 hrs after dosing. The relative abundance of clemizole and its metabolites in plasma were measured in samples obtained from 10 patients treated with clemizole alone, and from 3 patients who participated in the subcomponent evaluating the effect of ritonavir co-administration, by LC/MS analysis as described below.

***In vitro HCV replication assay*.** The plasmid FL-J6/JFH-5'C19Rluc2AUbi, which consists of the full-length HCV genome and expresses the *Renilla* luciferase (Tscherne et al., 2006), was a gift from Charles M. Rice. In vitro transcription of HCV RNA was performed as described with minor

modifications (Einav et al., 2010). Briefly, Huh 7.5 cells were maintained in DMEM (Gibco) supplemented with 1% L-glutamine (Gibco), 1% penicillin, 1% streptomycin (Gibco), 1x nonessential amino acids (Gibco) and 10% FBS (Omega Scientific). Electroporation was performed by mixing 5 µg of RNA with 400 µL of ice-cold PBS containing washed Huh 7.5 cells at a density of 1.5 x 10^7 cells/mL. The mixture was immediately pulsed (0.82 kV, five 99 µs pulses) with a BTX-830 electroporator. After a 10 min recovery at 25 °C, pulsed cells were diluted into 10 ml of pre-warmed growth medium. Cells were passaged, their luciferase activity verified, and seeded in 96-well plates (2×10^4cells/well) 1 day prior to addition of the inhibitory compounds. Cells were grown in 3 replicates in the presence of serial dilutions of the inhibitory compounds. Untreated cells with or without corresponding concentrations of DMSO were used as negative controls. 48 hour after treatment with the inhibitory compounds, cells were subjected to Alamar Blue-based viability assays and luciferase assays.

Viability Assay and Luciferase Assay. Cell viability was assessed by incubation with 10% Alamar Blue Reagent (Invitrogen) for 2 hours, the absorbance was measured at 570 nm and 630 nm with a plate reader (TECAN M1000), and viability is determined by comparing the $A_{570} - A_{630}$. Luciferase activity was measured using the *Renilla* luciferase kit (Promega) after assessing cell viability. The cells were washed with ice-cold PBS and lysed with 20 µL of ice-cold *Renilla* lysis buffer (Promega). We injected 40 µL of the *Renilla* luciferase assay buffer containing assay substrate and measured luciferase activity with a 4 sec integration using a plate reader. All experiments were done at least four times, and at least 3 replicates were performed each time.

Analysis of the drug synergy data. The in vitro drug efficacy data were analyzed using the The MacSynergy II program (kindly provided by M. N. Prichard) according to the Bliss independence model (Pritchard et al., 1992) (Prichard and Shipman, 1990). The effect of a drug

JPET Fast Forward. Published on November 8, 2012 as DOI: 10.1124/jpet.112.198697
This article has not been copyedited and formatted. The final version may differ from this version.

combination is determined by subtracting the experimental values from theoretical additive values (Pritchard et al., 1992). A 3-dimensional differential surface plot is used to evaluate the interaction between the tested drugs. Synergy is indicated if the plot peaks above a theoretical additive plane, and antagonism is indicated if depressions are formed below this plane (Prichard and Shipman, 1990). The data sets with 4 replicates were assessed at the 95% confidence level for each experiment (Pritchard et al., 1992) (Prichard and Shipman, 1990) (Prichard and Shipman, 1996). Synergy (volume under the curve) and log volume were calculated. As suggested (Pritchard et al., 1992), these data sets are interpreted according to the follow rules: volumes of synergy or antagonism at values of <25 μM^2% are insignificant, 25–50 μM^2% are minor but significant, 50–100 μM^2% are moderate and probably important *in vivo*, and >100 μM^2% are strong and likely to be important *in vivo*.

Results

We first examined clemizole's pharmacokinetic profile in a commonly used, conventional mouse strain. Clemizole had an un-expectedly short plasma half-life (measured at 0.15 hr); it was very rapidly biotransformed into a glucuronide (M14) and a dealkylated metabolite (M12), and into a variety of lesser metabolites in C57BL/6J mice (**Figure 1)**. Although we previously demonstrated that the pattern of metabolism for several drugs could differ among inbred strains (Guo et al., 2006; Guo et al., 2007), two other inbred strains exhibited the same ultra-rapid rate of clemizole metabolism and produced the same metabolites as C57BL/6J mice (**Supplemental Figure 1**). Then, the pattern of clemizole metabolism in TK-NOG mice with 'humanized livers' was compared with that in control mice with the same genetic background. Based upon the human albumin concentration (range 1.3 to 7.0 mg/ml) in their sera, the extent of liver humanization ranged from 13-70%. The relative amount of clemizole and 6 metabolites in plasma 30 min after administration of a single (25 mg/kg PO) dose of clemizole was measured

(**Table I**). The relative amounts of 3 metabolites did not significantly differ between control and humanized mice ($p>0.3$). However, 'humanized' TK-NOG mice had a substantially larger amount of metabolite **M1** in their plasma (2.2 fold, $p<0.0004$); along with a significantly increased level of M6 (1.5 fold, $p<0.049$), and a decreased amount of M14 (0.68 fold, $p<0.046$) in their plasma. Since these livers were only partially humanized, the remnant murine liver was also rapidly metabolizing this drug. However, by focusing on the differences in the drug metabolites that were produced by the humanized and conventional murine livers, drug metabolites that will predominate in humans could be identified. This data indicated that M1 and M6 could be important metabolites in humans, and that clemizole metabolism in humans and mice could differ.

After the murine studies were completed, plasma samples were obtained from ten human subjects after administration of a single (100 mg P.O.) dose of clemizole (**Figure 1**). Clemizole had a much longer plasma half-life (measured at 3.4 hrs) in humans, and a very different pattern of drug metabolites relative to mice. Clemizole was rapidly converted to a single major metabolite (M1), which accounted for 55% of all drug and metabolites present in human plasma. The area under the concentration time curve (**AUC**) (0-24 hr) is calculated to assess the relative level of drug or metabolite exposure over time. Comparison of the AUCs (0-24 hr) calculated for each metabolite indicates that mice and humans have very different levels of exposure to the major drug metabolites (**Table 2**). While M1 and M6 account for 77% of human drug metabolite exposure; they account for only 6% of murine drug metabolite exposure. In contrast, M12 and M14 account for 77% of mouse drug metabolite exposure, but only 2% of human metabolite exposure. The human metabolic profile was consistent with that observed in the humanized mice, which had indicated that the pathways mediating M1 and M6 production would be important.

JPET Fast Forward. Published on November 8, 2012 as DOI: 10.1124/jpet.112.198697
This article has not been copyedited and formatted. The final version may differ from this version.

Clemizole metabolism in rodents and humans. A detailed *in vitro* characterization of the pathways for clemizole metabolism in rodents and humans was performed as described in the supplement (**Supplemental Figures 2-3** and **Supplemental Tables 1-3**), and the inter-species differences are summarized in **Figure 1B**. In human liver, clemizole is primarily converted an intermediate A, which can be oxidized by several CYP450 enzymes (CYP3A4, CYP2C19 or CYP2D6) to M1. CYP3A4, which is the most abundantly expressed CYP450 enzyme in human liver, mediates the majority of this drug biotransformation reaction. The role of CYP3A4 is confirmed by the ability of ritonavir, which is an inhibitor of CYP3A4 activity, to inhibit clemizole metabolism *in vitro* (**Figure S4**). In contrast, a different type (CYP2C-like) of aromatic oxidation reaction produces the rodent-predominant metabolites (M12, M14 and M15), which is the dominant pathway for clemizole metabolism in rodent liver.

Predicting a human DDI. We wanted to determine if studies using humanized TK-NOG mice could prospectively predict whether a potential DDI involving clemizole would occur. Ritonavir is a CYP3A4 inhibitor, that has been co-administered with other drugs to increase their duration of action (Hsu et al., 1998). Given the identified pathways for clemizole metabolism in human liver, it was possible that ritonavir-mediated inhibition of CYP3A4 could alter clemizole pharmacokinetics. We hypothesized that if a DDI of this type occurred in the humanized mice, a similar type of DDI would be observed in human patients. Therefore, clemizole was administered to eight humanized TK-NOG mice with or without ritonavir co-administration, and clemizole metabolites were analyzed in plasma samples. Ritonavir co-administration decreased the amount of the human-predominant clemizole metabolites (M1 and M6, $p<0.005$) (**Figure 2**). The concentration of M12, a mouse predominant metabolite was also decreased by ritonavir co-administration, while the concentrations of two other metabolites (M14 and M15) that are produced by a mouse-specific biotransformation reaction were not altered. We have previously demonstrated that chimeric TK-NOG mice can metabolize debrisoquine to 4-OH-debrisoquine,

which is a human predominant route of drug metabolism that is catalyzed by CYP2D6 (Hasegawa et al., 2011). Ritonavir co-administration did not alter the CYP2D6-mediated conversion of debrisoquine to 4-OH debrisoquine in 6 humanized TK-NOG mice analyzed (p-value>0.5) (**Figure 2**). These results demonstrate that ritonavir co-administration specifically decreased the production of human CYP3A4-specific metabolites of clemizole, and indicate that a DDI could occur if ritonavir was co-administered with clemizole in human subjects.

Since increasing the time that an HCV-infected individual maintains an effective plasma clemizole concentration could have a therapeutic benefit, a pilot clinical study was performed to determine if ritonavir co-administration would increase plasma clemizole levels after dosing. Three HCV infected individuals were treated with clemizole (100 mg PO) alone, and on a separate day with clemizole (100 mg PO) and ritonavir (100 mg PO, one hour before clemizole administration). The plasma clemizole concentration was measured over a 12 hr period following both treatments. Ritonavir co-administration increased the AUC(0-12 hr) for clemizole in all 3 treated individuals (by 22, 38 and 89%, respectively) (**Figure 3**). Although ritonavir co-administration had a limited effect in the first patient, ritonavir co-administration substantially increased the Cmax and AUC for clemizole in patients 2 and 3. Thus, the humanized TK-NOG mouse results correctly predicted that a DDI would occur between ritonavir and clemizole, and this could be exploited to improve the efficacy of clemizole treatment for HCV infection.

Clemizole M1 metabolite has anti-viral activity. Since high levels of M1 were present in human plasma, it was of importance to determine whether this metabolite had anti-viral activity. Clemizole has recently been shown to have a synergistic inhibitory effect on HCV replication *in vitro* when combined with protease inhibitors (Einav et al., 2010). Therefore, the effect of the M1 metabolite, either alone or in combination with a protease inhibitor (boceprevir) that was recently approved for treatment of HCV (Bacon et al., 2011) (Poordad et al., 2011), was measured using

JPET Fast Forward. Published on November 8, 2012 as DOI: 10.1124/jpet.112.198697
This article has not been copyedited and formatted. The final version may differ from this version.

an *in vitro* luciferase reporter-linked HCV replication assay. When M1 was combined with boceprevir, their combined antiviral effect in this assay was significantly more potent than the theoretical additive effects of either drug alone (**Figure 4)**. The calculated synergy volume was 101 $\mu M^2\%$; which (according the established criteria (Pritchard et al., 1992)) is indicative of strong synergy that is likely to be important *in vivo*. There was no evidence of antiviral antagonism at any of the tested doses; and no cellular toxicity was noted after incubation with either drug alone, nor was cytotoxicity increased after exposure to the drug combinations. Thus, the observed synergy between boceprevir and M1 is specific, and it does not reflect a synergistic toxicity arising from the drug combination. Although the level of synergy observed with M1 was less than that obtained with clemizole (synergy volume 230 $\mu M^2\%$) (Figure 4), these results indicate that clemizole's major metabolite has significant anti-viral activity.

Discussion

Differences between the rodent and human pathways used for metabolism of a candidate medication are not rare, which is why animal testing results have not always accurately predicted human pharmacokinetic parameters or the drug metabolism pathways for a candidate medication (Anderson et al., 2009; Leclercq et al., 2009; Walker et al., 2009). Similarly, the results from *in vitro* analyses using human hepatocytes or microsomal preparations have correctly predicted the *in vivo* human metabolite profile for about half (46-65%) of the 48 tested compounds (Dalvie et al., 2009). This study indicates how the use of humanized TK-NOG mice can enable human-predominant drug metabolites to be identified prior to human drug exposure. Although chimeric mice have both human and murine liver tissue, human drug metabolites could be predicted by identifying the differentially abundant metabolites produced in chimeric mice (relative to conventional mice). However, the variable extent of liver humanization (13-70%) (**Supplemental Table 4**) in the chimeric mice analyzed here could complicate the analysis

of other drugs; especially when the pathways for murine and human drug metabolism are not as divergent as in the case examined here. The remaining mouse liver could produce metabolites that could confound toxicologic analyses performed with these chimeric mice. Therefore, methods are being developed to increase the extent of liver humanization that is obtained with this model system, which should improve the results obtained using humanized TK-NOG mice. Since three different inbred strains produced the same pattern of clemizole metabolites, there is a common murine (strain-independent) pattern of clemizole metabolism, which differs from the pathways used in humans. The inter-species differences in clemizole metabolism highlight the difficulties in using data obtained from conventional rodent species to predict human drug metabolism, and consequently, potential drug-induced toxicity. For clemizole, if toxicities were caused by the human predominant metabolite M1, toxicology testing in rodents would provide a false assurance of drug safety. Similarly, rodent testing could raise a false drug safety concern if a rodent-predominant (M12, M14) metabolite or reactive intermediate B caused toxicity. Although some form of human testing is always required for assessment of a candidate drug, the information obtained from analyses performed in chimeric mice prior to human testing can be quite informative. The identified differences between the rodent and human pathways for clemizole metabolism assume an increased importance, since the major human clemizole metabolite had synergistic anti-HCV activity *in vitro*, which could extend the anti-viral activity of clemizole when administered in combination with the recently approved HCV protease inhibitors. As demonstrated here, analyses in chimeric mice can reveal whether pre-clinical toxicity testing in animal species has adequately covered the metabolites that will be formed in humans. Although the interaction of ritonavir and clemizole provides a straightforward example, this study also demonstrates how chimeric mice can be used to assess whether a potential DDI is likely to occur.

Our analysis indicates that CYP3A4 plays a major role in clemizole metabolism. We previously

demonstrated that there was abundant human CYP3A4 protein expression in the livers of chimeric TK-NOG mice (Hasegawa et al., 2011). Although the effect that genetic differences in CYP3A enzymes have on clemizole metabolism remains to be determined, any compound that is metabolized by CYP3A4 is usually also a CYP3A5 substrate. However, the high frequency of inactivating CYP3A5*3 alleles in Caucasians (up to 90%) and Asians (up to 80%) makes it likely that CYP3A5 may have a lesser role in clemizole metabolism (Lamba et al., 2002) (Xie et al., 2004). It is more likely that inter-individual variability in CYP3A4 expression is responsible for the variable affect of ritonavir on the pharmacokinetic profiles in these 3 randomly selected Caucasian individuals.

Consistent with the results obtained from analysis of other drugs (Dalvie et al., 2009), the data in **Table 2** indicates that the *in vitro* results (microsomes or hepatocytes) did not correctly predict the *in vivo* profile of clemizole metabolism. Since the rodent *in vitro* systems could not even predict how clemizole would be metabolized *in vivo* in rodents, it would have been very difficult to use human *in vitro* data to predict the clemizole metabolites that would be produced in human subjects. However, there are limiting factors affecting the use of these chimeric mice for human-specific pharmacokinetic and toxicologic studies. (i) These mice cannot be used to analyze immune-mediated drug toxicities because they are immunocompromised. (ii) They cannot be used to identify extra-hepatic human-specific factors affecting drug metabolism or clearance. (iii) Since we do not know the extent of biliary tract humanization in these chimeric mice, we do not know if they can be used to predict the clearance of drugs in humans that depend upon human-specific transporter-mediated hepatobiliary clearance. Until we know the extent of biliary tract humanization, we do not know whether the potential for drugs [e.g. bosentan (Fattinger et al., 2001)] to cause cholestatic liver toxicity in humans can be evaluated in these mice. Despite these limitations, this example demonstrates how the use of humanized mice can enhance our ability to predict human drug metabolism and the occurrence of a DDI for

a candidate medication. As has occurred with other medications (Hsu et al., 1998), ritonavir co-administration could be used to increase the anti-HCV efficacy of clemizole. Although this is only one example, it indicates that it is likely that the use of chimeric mice could improve the quality of pre-clinical drug assessment.

Acknowledgements

We thank Wenjin Yang and Eiger BioPharmaceuticals, Inc. for providing the clinical samples used in this study.

Author Contributions

Performed experiments: Nishimura, Hu, Suemizu, Wu, Elazar, Liu, Idilman, Yurdaydin, Angus, Stedman and Murphy

Wrote Paper: Hu, Peltz, Glenn

Data Analysis: Zheng, Fitch

Designed experiments: Nakamura, Nomura and Chen

Participated in the design of the studies: Glenn, Peltz

References

Anderson S, Luffer-Atlas D and Knadler MP (2009) Predicting circulating human metabolites: how good are we? *Chem Res Toxicol* **22**:243-256.

Azuma H, Paulk N, Ranade A, Dorrell C, Al-Dhalimy M, Ellis E, Strom S, Kay MA, Finegold M and Grompe M (2007) Robust expansion of human hepatocytes in Fah-/-/Rag2-/-/Il2rg-/- mice. *Nature Biotechnology* **25**:903-910.

Bacon BR, Gordon SC, Lawitz E, Marcellin P, Vierling JM, Zeuzem S, Poordad F, Goodman ZD, Sings HL, Boparai N, Burroughs M, Brass CA, Albrecht JK and Esteban R (2011) Boceprevir for previously treated chronic HCV genotype 1 infection. *N Engl J Med* **364**:1207-1217.

Bissig K-D, Wieland SF, Tran P, Isogawa M, Le TT, Chisari FV and Verma IM (2010) Human liver chimeric mice provide a model for hepatitis B and C virus infection and treatment. *Journal of Clinical Investigation* **120**:650-653.

Bode C (2010) The nasty surprise of a complex drug-drug interaction. *Drug Discov Today* **15**:391-395.

Chen AA, Thomas DK, Ong LL, Schwartz RE, Golub TR and Bhatia SN (2011) Humanized mice with ectopic artificial liver tissues. *Proc Natl Acad Sci U S A*.

Dalvie D, Obach RS, Kang P, Prakash C, Loi CM, Hurst S, Nedderman A, Goulet L, Smith E, Bu HZ and Smith DA (2009) Assessment of three human in vitro systems in the generation of major human excretory and circulating metabolites. *Chem Res Toxicol* **22**:357-368.

de Jong YP, Rice CM and Ploss A (2010) New Horizons for Studying human hepatotropic infections. *The Journal of Clinical Investigation* **120**:650-653.

De Serres M, Bowers G, Boyle G, Beaumont C, Castellino S, Sigafoos J, Dave M, Roberts A, Shah V, Olson K, Patel D, Wagner D, Yeager R and Serabjit-Singh C (2011) Evaluation of a chimeric (uPA+/+)/SCID mouse model with a humanized liver for prediction of human metabolism. *Xenobiotica* **41**:464-475.

Einav S, Gerber D, Bryson PD, Sklan EH, Elazar M, Maerkl SJ, Glenn JS and Quake SR (2008) Discovery of a hepatitis C target and its pharmacological inhibitors by microfluidic affinity analysis. *Nat Biotechnol* **26**:1019-1027.

Einav S, Sobol HD, Gehrig E and Glenn JS (2010) The hepatitis C virus (HCV) NS4B RNA binding inhibitor clemizole is highly synergistic with HCV protease inhibitors. *J Infect Dis* **202**:65-74.

Fattinger K, Funk C, Pantze M, Weber C, Reichen J, Stieger B and Meier PJ (2001) The endothelin antagonist bosentan inhibits the canalicular bile salt export pump: a potential mechanism for hepatic adverse reactions. *Clin Pharmacol Ther* **69**:223-231.

Guengerich FP and MacDonald JS (2007) Applying mechanisms of chemical toxicity to predict drug safety. *Chem Res Toxicol* **20**:344-369.

Guo YY, Liu P, Zhang X, Weller PMM, Wang J, Liao G, Zhang Z, Hu J, Allard J, Shafer S, Usuka J and Peltz G (2007) In vitro and In silico Pharmacogenetic Analysis in Mice. *Proceedings of the National Academy of Sciences* **104**:17735-17740.

Guo YY, Weller PF, Farrell E, Cheung P, Fitch B, Clark D, Wu SY, Wang J, Liao G, Zhang Z, Allard J, Cheng J, Nguyen A, Jiang S, Shafer S, Usuka J, Masjedizadeh M and Peltz G (2006) In Silico Pharmacogenetics: Warfarin Metabolism. *Nature Biotechnology* **24**:531-536.

Hasegawa M, Kawai K, Mitsui T, Taniguchi K, Monnai M, Wakui M, Ito M, Suematsu M, Peltz G, Nakamura M and Suemizu H (2011) The reconstituted 'humanized Liver' in TK-NOG mice is mature and functional. *Biochem Biophys Res Commun* **405**:405-410.

Hsu A, Granneman GR and Bertz RJ (1998) Ritonavir. Clinical pharmacokinetics and interactions with other anti-HIV agents. *Clinical Pharmacokinetics* **35**:275-291.

Ito M, Hiramatsu H, Kobayashi K, Suzue K, Kawahata M, Hioki K, Ueyama Y, Koyanagi Y, Sugamura K, Tsuji K, Heike T and Nakahata T (2002) NOD/SCID/gamma cnull mouse: an excellent recipient mouse model for engraftment of human cells. *Blood* **100**:3175-3182.

Kamimura H, Nakada N, Suzuki K, Mera A, Souda K, Murakami Y, Tanaka K, Iwatsubo T, Kawamura A and Usui T (2010) Assessment of chimeric mice with humanized liver as a tool for predicting circulating human metabolites. *Drug Metab Pharmacokinet* **25**:223-235.

Katoh M, Sawada T, Soeno Y, Nakajima M, Tateno C, Yoshizato K and Yokoi T (2007) In vivo drug metabolism model for human cytochrome P450 enzyme using chimeric mice with humanized liver. *Journal of Pharmaceutical Sciences* **96**:428-437.

Katoh M and Yokoi T (2007) Application of Chimeric Mice with Humanized Liver for Predictive ADME. *Drug Metabolism Reviews* **39**:145-157.

Lamba JK, Lin YS, Schuetz EG and Thummel KE (2002) Genetic contribution to variable human CYP3A-mediated metabolism. *Adv Drug Deliv Rev* **54**:1271-1294.

Leclercq L, Cuyckens F, Mannens GS, de Vries R, Timmerman P and Evans DC (2009) Which human metabolites have we MIST? Retrospective analysis, practical aspects, and perspectives for metabolite identification and quantification in pharmaceutical development. *Chem Res Toxicol* **22**:280-293.

Lootens L, Van Eenoo P, Meuleman P, Leroux-Roels G and Delbeke FT (2009) The uPA(+/+)-SCID mouse with humanized liver as a model for in vivo metabolism of 4-androstene-3,17-dione. *Drug Metab Dispos* **37**:2367-2374.

Meuleman P, Libbrecht L, De V, de H, Gevaert K, Vandekerckhove J, Roskams T and Leroux R (2005) Morphological and biochemical characterization of a human liver in a u PA-SCID mouse chimera. *Hepatology* **41**:847-856.

Poordad F, McCone J, Jr., Bacon BR, Bruno S, Manns MP, Sulkowski MS, Jacobson IM, Reddy KR, Goodman ZD, Boparai N, DiNubile MJ, Sniukiene V, Brass CA, Albrecht JK and Bronowicki JP (2011) Boceprevir for untreated chronic HCV genotype 1 infection. *N Engl J Med* **364**:1195-1206.

Pozo OJ, Van Eenoo P, Deventer K, Lootens L, Grimalt S, Sancho JV, Hernandez F, Meuleman P, Leroux-Roels G and Delbeke FT (2009) Detection and structural investigation of metabolites of stanozolol in human urine by liquid chromatography tandem mass spectrometry. *Steroids* **74**:837-852.

Prichard MN and Shipman C, Jr. (1990) A three-dimensional model to analyze drug-drug interactions. *Antiviral Res* **14**:181-205.

Prichard MN and Shipman C, Jr. (1996) Analysis of combinations of antiviral drugs and design of effective multidrug therapies. *Antivir Ther* **1**:9-20.

Pritchard MN, Prichard LE and Shipman C, Jr. (1992) MacSynergy II version 1.0 user's manual, in, University of Michigan, Ann Arbor.

Smith DA and Obach RS (2009) Metabolites in safety testing (MIST): considerations of mechanisms of toxicity with dose, abundance, and duration of treatment. *Chem Res Toxicol* **22**:267-279.

Tateno C, Yoshizane Y, Saito N, Kataoka M, Utoh R, Yamasaki C, Tachibana A, Soeno Y, Asahina K, Hino H, Asahara T, Yokoi T, Furukawa T and Yoshizato K (2004) Near Completely Humanized Liver in Mice Shows Human-Type Metabolic Responses to Drugs. *American Journal of Pathology* **165**:901-912.

Tscherne DM, Jones CT, Evans MJ, Lindenbach BD, McKeating JA and Rice CM (2006) Time- and temperature-dependent activation of hepatitis C virus for low-pH-triggered entry. *J Virol* **80**:1734-1741.

Vyse TJ, Rozzo SJ, Drake CG, Izui S and Kotzin BL (1980) Control of Multiple Autoantibodies Linked with a Lupus Nephritis Susceptibility Locus in New Zealand Black Mice 1. *Journ of Immunology*.

Walker D, Brady J, Dalvie D, Davis J, Dowty M, Duncan JN, Nedderman A, Obach RS and Wright P (2009) A holistic strategy for characterizing the safety of metabolites through drug discovery and development. *Chem Res Toxicol* **22**:1653-1662.

Xie HG, Wood AJ, Kim RB, Stein CM and Wilkinson GR (2004) Genetic variability in CYP3A5 and its possible consequences. *Pharmacogenomics* **5**:243-272.

Yoshizato K and Tateno C (2009) In vivo modeling of human liver for pharmacological study using humanized mouse. *Expert Opin Drug Metab Toxicol* **5**:1435-1446.

Zhang L, Reynolds KS, Zhao P and Huang SM (2010) Drug interactions evaluation: an integrated part of risk assessment of therapeutics. *Toxicol Appl Pharmacol* **243**:134-145.

Footnotes

[a] This work was supported by a Transformative RO1 award from the National Institutes of Health National Institute of Diabetes and Digestive and Kidney Diseases to G.P [1R01DK090992-01]. J.G and B.M were partially supported by an award from the National Institutes of Health National Institute Allergy and Infectious Diseases [R42 AI088793].

*These authors contributed equally to this work

Address reprint requests to: Gary Peltz, Stanford University School of Medicine 300 Pasteur Drive L232 Stanford CA 94305; gpeltz@stanford.edu

Disclosure

One author (JG) has an equity interest in, and three authors (JG, GP, BM) are consultants for Eiger BioPharmaceuticals and/or Eiger Group International, which are developing clemizole for HCV treatment.

Figure Legends

Figure 1. (A) Clemizole metabolism in mice and humans. The top graphs show the measured plasma clemizole concentration at the indicated times after a single oral dose of clemizole was administered to three C57BL/6 mice (25 mg/kg) or 10 human subjects (100 mg). While clemizole was rapidly metabolized in mice (measured half-life 0.15 hr), its measured half-life in humans was 3.4 hr. The bottom graphs show the relative normalized abundance of clemizole and metabolites in plasma at the indicated time after dosing. In mice, clemizole was rapidly metabolized to 2 major (M12 and M14) metabolites, but only minimal amounts of M1 or M6 were produced; while in humans, clemizole was converted to two predominant metabolites (M1 and M6). (**B)** The structure of clemizole and the pathways for production of its metabolites are shown. In humans, clemizole is converted to intermediate 'A' by any of a number of CYP450s. Then, CYP3A4, CYP2C19 and CYP2D6 can further oxidize this intermediate to M1; while in the presence of CYP2C9 or CYP1A2, M2 is generated, but they cannot produce M1. Cyp2C9 appears to be the only source of M4, which is a minor metabolite in humans. The structures of the major human (M1, M6) and rodent (M12, M14) plasma metabolites are highlighted.

Figure 2. Top panel: Six humanized TK-NOG mice were first dosed with clemizole alone (25 mg/kg PO), and then with clemizole (25 mg/kg PO) and ritonavir (20 mg/kg PO). The amount of 6 different clemizole metabolites in plasma was measured at 30 minutes after dosing. The plasma concentrations of the human-predominant M1 and M6 metabolites were significantly decreased by ritonavir co-administration, as were the concentrations of M2 and M12, while that of M14 and M15 was unchanged. Bottom panel: Five humanized TK-NOG mice were first dosed with debrisoquine alone (10 mg/kg PO), and then with Debrisoquine (10 mg/kg PO) and ritonavir (20 mg/kg PO). The amount of its main metabolite, 4-OH-debrisoquine was measured in plasma 2 hrs after dosing. The relative amount of 4-OH debrisoquine was not significantly

changed by ritonavir co-administration.

Figure 3. Three HCV infected individuals were first administered clemizole alone (100 mg PO), and then with clemizole (100 mg PO) and ritonavir (100 mg PO BID). The amount of clemizole in the plasma was measured over a 12 hr period after dosing.

Figure 4. Differential surface plot of the synergistic anti-HCV effect of boceprevir with either clemizole (top) or the M1 metabolite of clemizole (bottom). The 3-dimensional plot represents the differences between the actual anti-viral effects and the theoretical additive effects at the indicated concentrations for the 2 compounds tested. Only statistically significant (95% CI) differences between the 2 compounds were considered at any given concentration. Peaks above the theoretical additive plane indicate synergy, whereas depressions below it indicate antagonism. The colors indicate the level of synergy or antagonism. Both clemizole and the M1 metabolite exhibit a substantial synergistic anti-viral effect with boceprevir.

JPET Fast Forward. Published on November 8, 2012 as DOI: 10.1124/jpet.112.198697
This article has not been copyedited and formatted. The final version may differ from this version.

Table 1. Clemizole (25 mg/kg PO) was administered to eight control NOG mice (C1-8) and eight TK-NOG mice with 'humanized livers' (Hu m1-8). The relative amounts of 6 metabolites and clemizole in plasma 30 min after dosing were measured. This table shows the human serum albumin (**hAlb**) concentration (mg/ml) in the humanized liver TK-NOG mice, and the relative abundances of clemizole metabolites in plasma. The ratio indicates the average amount of each metabolite in humanized TK-NOG mice divided by that in control mice. Although both groups had equivalent relative amounts of 3 metabolites (p-value>0.3), the 'humanized' mice had a significantly increased relative amount of the M1 and M6 metabolites, and a significantly decreased relative amount of M14.

	hAlb	**Clem**	**M1**	**M2**	**M6**	**M12**	**M14**	**M15**
C1		4.1	4.1	10.4	14.1	28.3	37.5	1.4
C2		5.5	3.2	8.1	12.9	37.9	31.2	1.2
C3		6.8	2.3	3.3	8	24	50.6	4.8
C4		3.1	3.1	8	9.3	20.5	39.3	16.7
C5		2.8	8	5.7	12.1	27.5	33.3	10.7
C6		6.03	5.49	20.00	10.19	28.78	28.50	1.01
C7		3.81	1.79	6.52	12.17	27.04	47.22	1.46
C8		4.53	6.43	11.38	10.17	25.76	40.71	1.02
Hu m1	4.2	1.8	8.9	13.6	8.3	20.6	39.8	6.9
Hu m2	1.5	4.4	7.1	8.3	13	29.6	35.5	2.4
Hu m3	1.6	5.3	7.9	9.2	16.8	32.1	26.9	1.8
Hu m4	2.2	4.3	7.1	14.2	5.9	14.8	48.5	5.2
Hu m5	2.7	3.6	13.1	10	26	29	16.5	1.8
Hu m6	1.3	6.25	12.25	18.24	23.10	26.37	12.33	1.46
Hu m7	7	8.75	10.73	18.66	21.30	28.86	9.59	2.12
Hu m8	1.6	7.02	9.04	13.59	19.92	28.77	20.69	0.97
Ratio		1.13	2.21	1.44	1.51	0.96	0.68	0.59
p-value		0.526	0.0004	0.095	0.049	0.659	0.046	0.389

JPET Fast Forward. Published on November 8, 2012 as DOI: 10.1124/jpet.112.198697
This article has not been copyedited and formatted. The final version may differ from this version.

Table 2. The AUC (0-24 hr) for exposure to clemizole and the major *in vivo* metabolites were calculated for C57BL/6 mice and for human subjects using the data presented in Figure 1. For comparison with the *in vitro* results, the % of the total identified metabolites present after clemizole was incubated with human, rat or mouse microsomes for 1 hr, or after incubation with rat or human hepatocytes for 30 minutes are shown.

% Total AUC			Microsomes		Hepatocytes		
Metabolite	**Human**	**Mouse**	**Human**	**Mouse**	**Rat**	**Human**	**Rat**
Clemizole	8.8	1.3	40	24	3	15	0
M1	54.9	4.7	35	2	4	39	0
M2	1.1	5.6	2	5	4	0.1	0
M4	1.1	2.9	5	3	5	4	0
M6	22.0	2.4	2	2	3	18	0
M9	8.8	0.3	3	19	37	4	1
M12	1.1	21.2	0.6	0	0	1	1
M14	1.1	55.8	0	0	0	10	5
M15	1.1	5.9	0	0	0	0	44

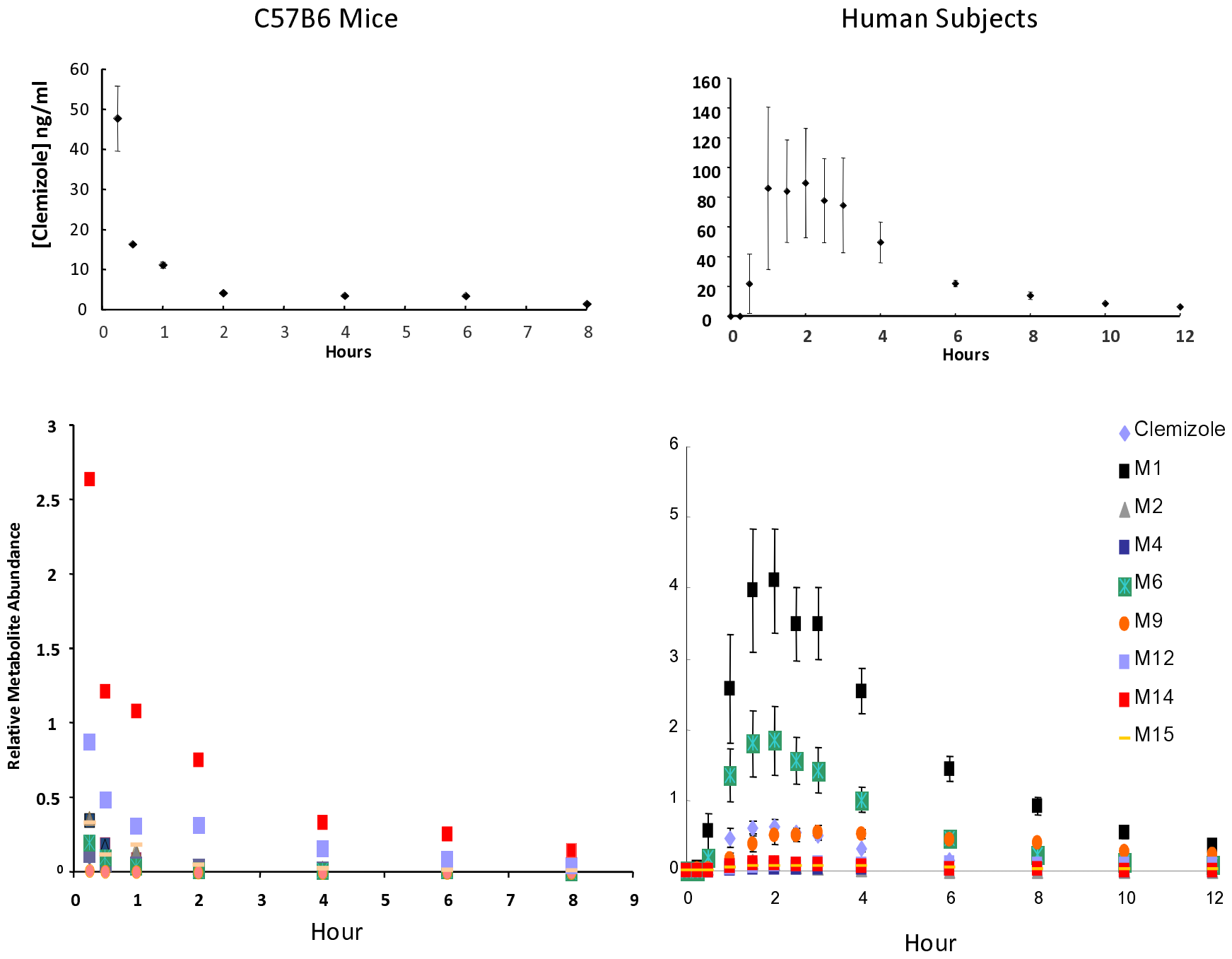

Fig 1A

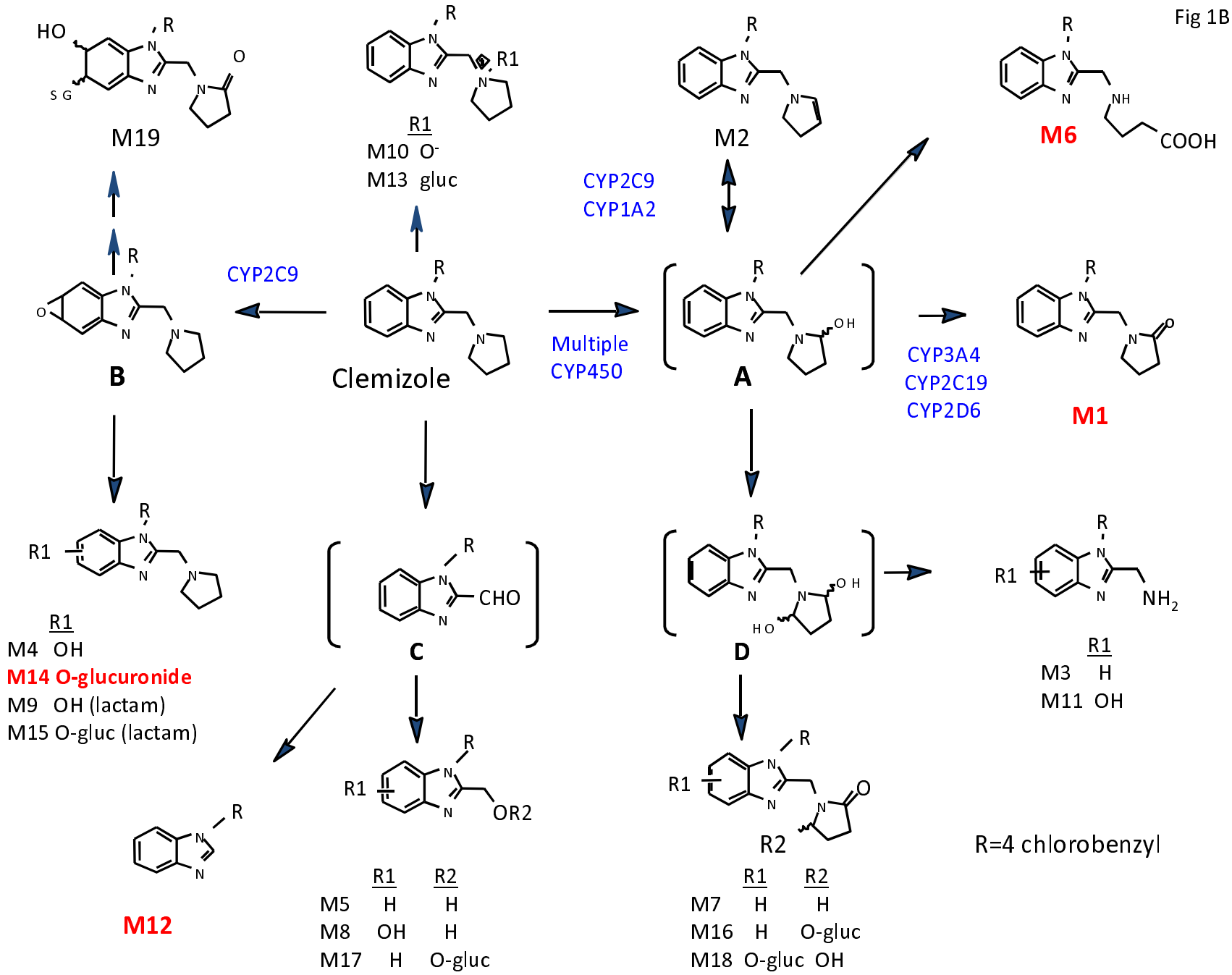

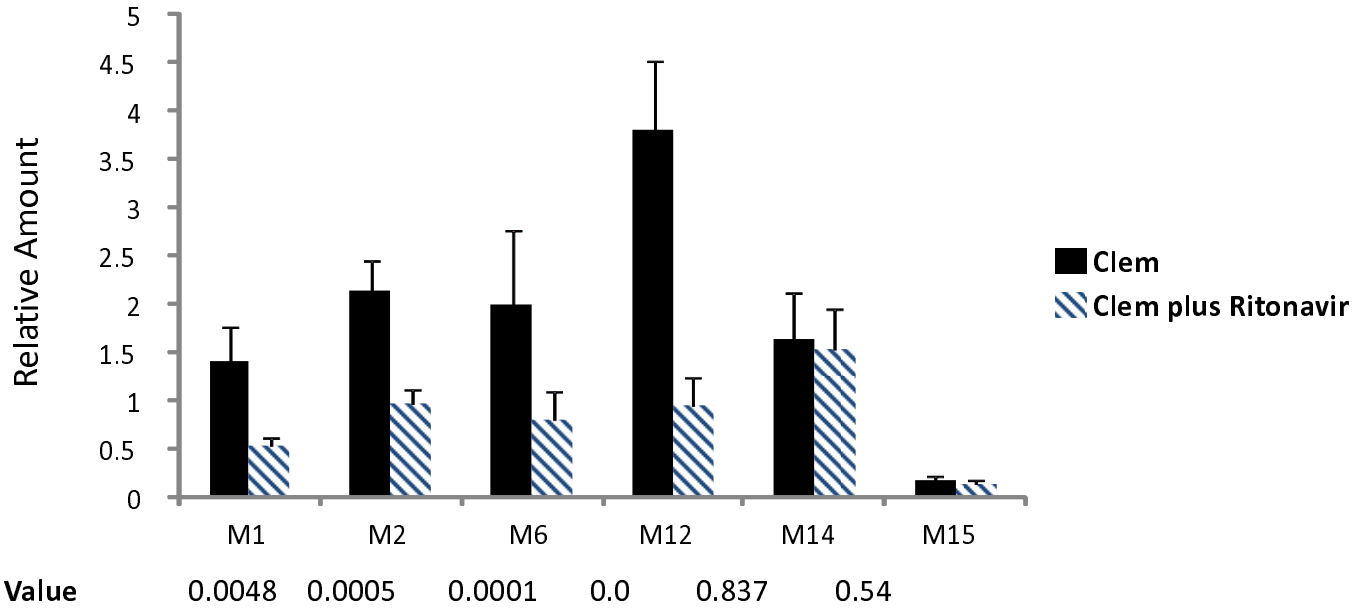

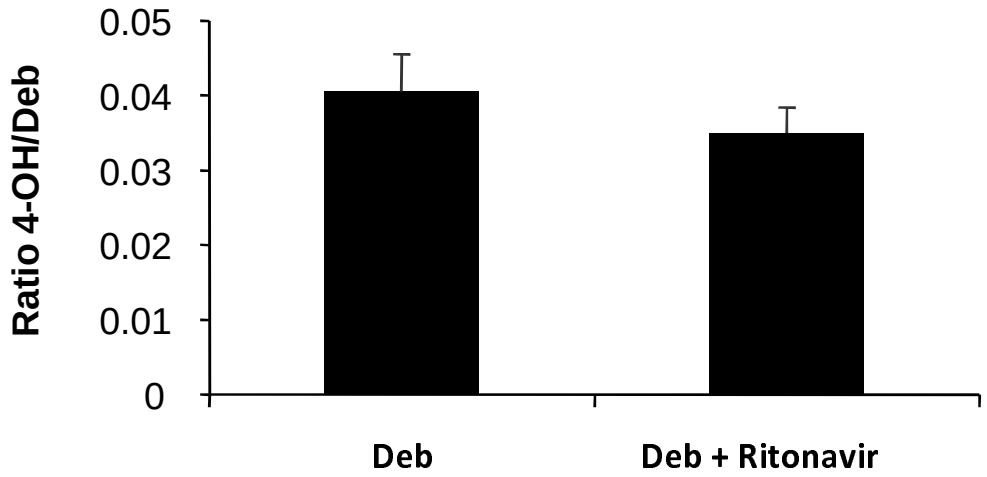

Fig 3

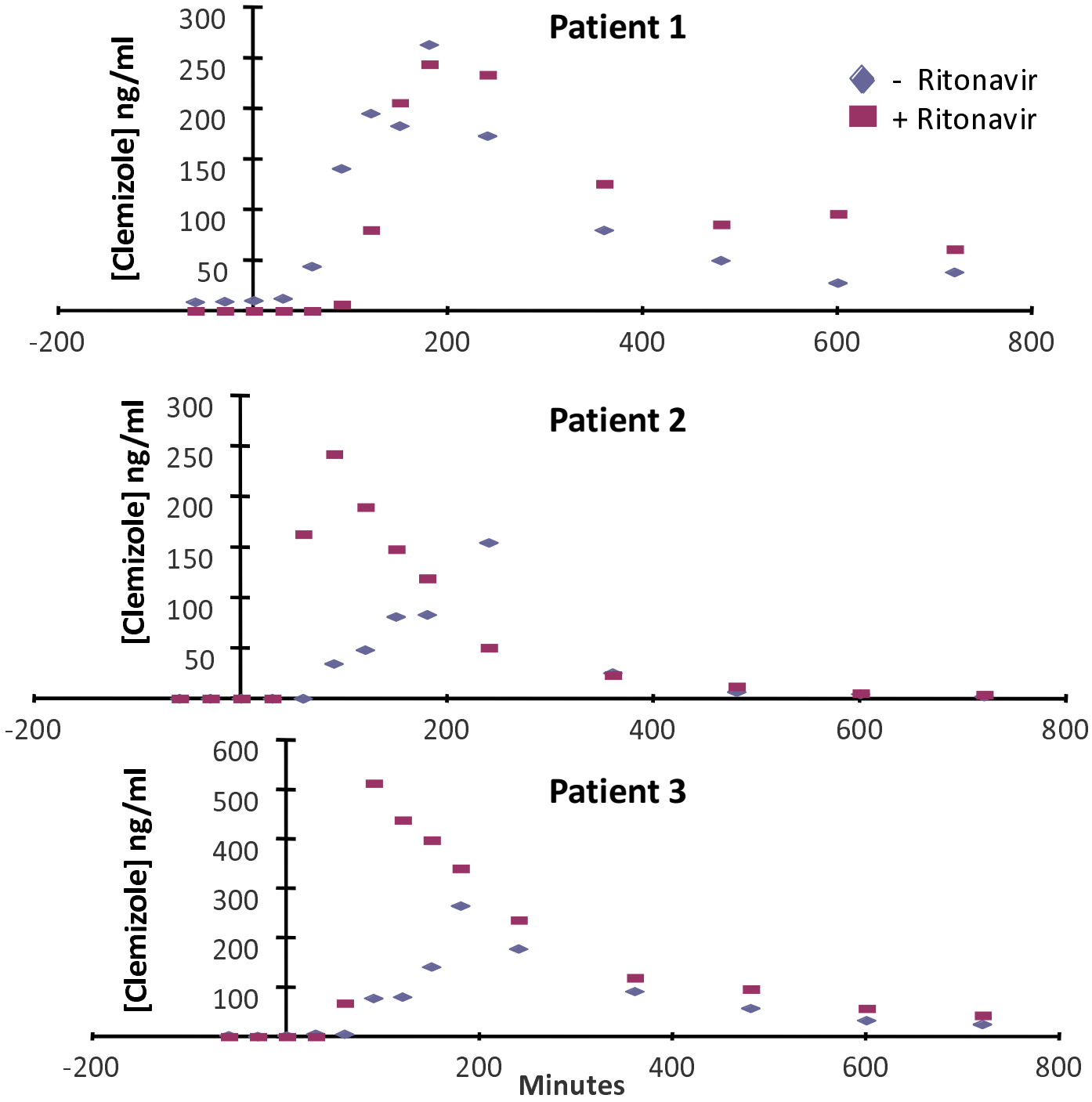

JPET Fast Forward. Published on November 8, 2012 as DOI: 10.1124/jpet.112.198697
This article has not been copyedited and formatted. The final version may differ from this version.

Fig 4

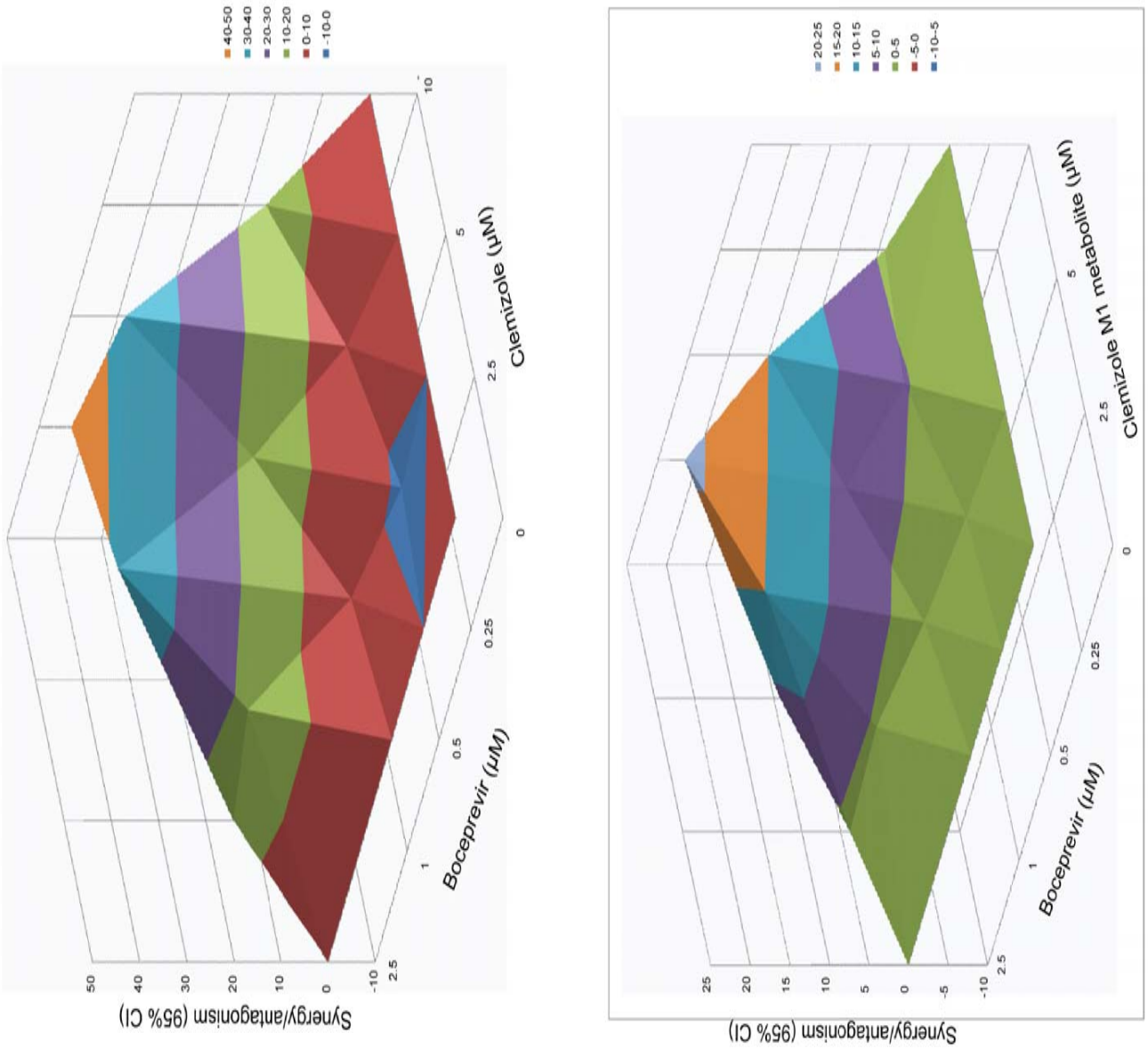

Supplemental Information

Using Chimeric Mice with Humanized Livers to Predict Human Drug Metabolism and a Drug-Drug Interaction

Toshiko Nishimura[1]*, Yajing Hu[1]*, Manhong Wu[1], Edward Pham[2], Hiroshi Suemizu[3], Menashe Elazar[2], Michael Liu[2], Ramazan Idilman[5], Cihan Yurdaydin[5], Peter Angus[6], Catherine Stedman[7], Brian Murphy[8], Jeffrey Glenn[2], Masato Nakamura[3], Tatsuji Nomura[3], Yuan Chen[4], Ming Zheng[1], William L. Fitch[1], and Gary Peltz[1#]

***In vitro* characterization of clemizole metabolism**. To characterize the metabolic pathways and the basis for the inter-species differences, a detailed *in vitro* analysis of clemizole metabolism was performed. First, the metabolites formed after clemizole was incubated with mouse rat and human microsomes were determined as described in the supplemental information. Clemizole exhibited much greater stability in human microsomes, where it is largely metabolized on the pyrrolidine ring to form one major metabolite, the lactam, **M1**. Clemizole is more rapidly metabolized by rodent microsomes to multiple different metabolites (**M8, M9**), but very little **M1** was formed (**Figure S2, Tables S1, S2**). Since intact liver cells can generate more complex metabolites, the profile of clemizole metabolites formed after incubation with human and rat hepatocytes was next characterized (**Table S2**). M1 was the major metabolite formed after incubation with human hepatocytes; and smaller amounts of M14 (the glucuronide of M4) and M6, which is a ring-opened pyrrolidine oxidation product, were also formed. However, rat hepatocytes produced a very different pattern of clemizole metabolites; M15 (the glucuronide of M9) was the major metabolite and lesser amounts of other Phase 2 metabolites (M16-M19) were also formed. It is noteworthy that none of the rodent *in vitro* systems identified the major clemizole metabolites (M12, M14) that were produced by mice *in vivo*. Then, CYP450 reaction phenotyping indicated that clemizole could be metabolized by a variety of human CYP450 enzymes (described in the supplement and **Figure S3).** Taken together, the recombinant CYP450 enzyme and microsome data indicate that in human liver

clemizole is primarily converted to intermediate 'A' (Figure 2). Then, several CYP450 enzymes (CYP3A4, CYP2C19 or CYP2D6) could further oxidize this intermediate to M1; while CYP2C9 or CYP1A2 can produce M2, but they cannot produce M1; and CYP2C9 appears to be the only source for M4. After considering the relative CYP450 abundance and other factors (Proctor et al., 2004), the extrapolated data indicate that CYP3A4 and CYP2C9 account for 53% and 30%, respectively, of the human Phase 1 metabolism of clemizole; while CYP2D6 and CYP2C19 each contribute to ~5-10% of clemizole metabolism. The ability of ritonavir, which is an inhibitor of CYP3A4 activity, to inhibit clemizole metabolism *in vitro* is consistent with these results, and indicates that CYP3A4 plays a major role in clemizole metabolism (**Figure S4**). M1 is the predominant human drug metabolite because CYP3A4 is the most abundantly expressed (60% of total) hepatic CYP450 enzyme (Danielson, 2002). Although rodent CYP450 phenotyping was not performed, clemizole metabolism in rodents must be dominated by a CYP2C-type of aromatic oxidation reaction that produces the rodent predominant metabolites (M12, M14 and M15) shown in Figure 2.

Analysis of the structure of clemizole metabolites. Clemizole has three sites that are susceptible to Cytochrome P450 oxidation: the pyrrolidine, the benzimidazole and the linker between them. The chlorobenzyl group is stable to metabolism. The metabolites were identified based on their collision-induced dissociation (CID) behavior in tandem mass spectrometry, accurate mass and retention time. Table S1 lists the structures and relevant LC/MS/MS information. Figure 2 shows the structures of clemizole and its metabolites, and its metabolic pathways. All metabolites had an observed accurate mass within 2.8 ppm of the predicted accurate mass. Clemizole fragments upon CID to yield a predominate ion at m/z 255, due to loss of pyrrolidine. This ion is moved to m/z 271 in the aromatic ring oxidized metabolites. Clemizole also has a major CID fragment at m/z 125 that represents the chlorobenzyl cation and is unchanged in all metabolites. The predominant metabolite produced by human

microsomes M1 had a molecular ion 14 Da greater than clemizole, and the m/z 125 fragment ion with CID, which indicated the oxidation had occurred on the pyrrolidine; As M1 had a longer retention time than clemizole in reverse phase LC, this metabolite, is identified as the lactam. M2 has a molecular weight 2 Da less than clemizole so it is drawn as the dehydro metabolite. The aminol metabolite A initially formed via alpha-oxidation in the pyrrolidine was not observed here; it may be unstable during LC/MS to produce M2; or it may be further oxidized to form M1, M3 or M6 *in vitro* and *in vivo*. M3 is the primary amine formed via further oxidation of A or M6 possibly through unstable intermediate B. In CID M3 loses ammonia predominately to give m/z 255. M4 and M10 are mono-hydroxylation metabolites. M4, with its indicative CID fragment moved to m/z 271 and a short retention time, is drawn with oxidation on the benzimidazole although the exact regiochemistry is not certain. M10 is drawn as the N-oxide as it's retention time is similar to clemizole and it's CID main indicative fragment is at m/z 256/257 (N-oxides typically lead to altered CID patterns including radical species (Fitch et al., 2007).) M5 with an even-to-odd mass shift (due to nitrogen loss) is drawn as the primary alcohol that could be formed by reduction of an aldehyde, which would initially form if bridgehead oxidation and loss of pyrrolidine occurred. M6 is an amino acid likely formed via further oxidation of the unstable metabolite A. M6 is of higher abundance in hepatocyte incubations and *in vivo*. M7 and M9 are isomeric doubly oxidized metabolites with a net increase of +30 Da. M7 has dual oxidations on the pyrrolidine ring with its indicative fragment at m/z 255 along with a dominant water loss fragment. M9 combines the features of M1 and M4 with its indicative fragment at m/z 271. M8 combines the features of M4 and M5 with the characteristic m/z 271 ion due to water loss. M11 combines the features of M3 and M4 with the indicative fragment at m/z 271. M12 is a metabolite mainly observed in vivo; it has a molecular formula consistent with a complete loss of the pyrrolidinylmethyl side chain possibly via further oxidation of M3 or M5.

The identification of metabolites produced in hepatocyte incubations was conducted with an LTQ Orbitrap so MS^3 data is listed for these metabolites. MS^3 is very useful for identifying Phase 2 metabolites because in the first stage of CID the glucuronide (or sulfate) is removed so the MS^3 spectrum of a Phase 2 metabolite is identical to the MS/MS spectrum of the corresponding Phase 1 metabolite. M13 is a glucuronide of the parent drug, which was only observed after incubation with human hepatocytes. It is likely a quaternary N-glucuronide of the pyrrolidine, a pathway that is often lacking in rodents (Chiu and Huskey, 1998). M14 has the $[M+H]^+$ consistent with a mono-oxidation and a glucuronidation. In MS/MS M14 gave rise to fragment ions at m/z 342 and 271 consistent with it being the glucuronide of M4. M15 has the $[M+H]^+$ consistent with a double-oxidation and a glucuronidation. In MS/MS M15 gave rise to fragment ions at m/z 356 and 271 consistent with it being the glucuronide of M9. M16 is a glucuronide of M7 with the characteristic m/z 255 fragment ion. M17 is an acyl glucuronide of M6. M18 is a minor rat-specific glucuronide of a triply oxidized phase 1 metabolite (not observed unconjugated). M19 is a rat-specific glutathione conjugate with a mass consistent with glutathione trapping from an arene oxide reactive intermediate on the pathway to M9.

Recombinant Cyp450 reaction data. The data shown in Figure S3 indicates that multiple CYP450 are involved in the clemizole metabolism. Clemizole was rapidly metabolized after incubation with CYP2C9, CYP2C19, CYP2D6, or CYP3A4; and with CYP1A2 to a lesser extent. After other factors such as CYP450 abundance and differences in intrinsic activity between the recombinant system and human liver microsomes are incorporated (Proctor et al., 2004), the extrapolated data indicates that CYP3A4 and CYP2C9, are the major CYP450 isoforms that could account for 53% and 30%, respectively, of the Phase 1 metabolism of clemizole; while CYP2D6 and CYP2C19 are each responsible for ~5-10% of clemizole metabolism. A more detailed structural (QTRAP MRM-EPI) analysis of metabolites produced after incubation with 10 uM clemizole confirms that multiple metabolites were formed after clemizole was incubated with

each of the different CYP isoforms (**Table S3**). CYP3A4 is primarily responsible for production of metabolites M1 and M2; CYP2C9 for M2 and M4; CYP2D6 for M1 and M2; CYP2C19 for M2; and CYP1A2 for M2 and M4. Taken together, this data indicates that in human liver clemizole is converted to intermediate A (Figure 2) *in vitro*. CYP3A4, CYP2C19 and CYP2D6 can further oxidize this intermediate to M1; while in the presence of CYP2C9 or CYP1A2, M2 is generated, but they cannot produce M1. Cyp2C9 appears to be the only source of M4.

Supplemental Materials and Methods

Chemicals and reagents. For *in vitro* and animal experiments, clemizole hydrochloride and omeprazole were purchased from Sigma (St. Louis, MO); ritonavir was purchased from Santa Cruz Biotechnology (Santa Cruz, CA). Pooled Human liver microsomes, male rat and mouse liver microsomes were purchased from BD Gentest (Woburn,MA). Cryopreserved human hepatocytes and recombinant CYP450 enzymes were purchased from BD Biosciences (San Jose, CA, USA). Rat hepatocytes were freshly isolated according to standard procedures. All other chemicals were purchased from commercial sources and were of the highest purity available.

Mouse pharmacokinetic studies. All animal experiments were performed using protocols approved by the Stanford Institutional Animal Care and Use Committee. Male C57BL6/J mice (8 weeks of age) were obtained from Jackson Labs and housed for 2 weeks prior to experimentation. NOG mice were obtained from In Vivo Sciences International (Sunnyvale, CA). Chimeric TK-NOG mice with humanized livers were prepared exactly as described (Hasegawa et al., 2011), except the Gancyclovir dose was increased to 25 mg/kg, which was administered 7 and 5 days prior to human liver cell transplantation. For transplantation, freshly isolated or cryopreserved human hepatocytes were obtained from Celsis In Vitro Inc. (Baltimore, MD) and

Life Technologies (Grand Island, NY). The characteristics of the human hepatocyte donors are described in **Table S4**. The pharmacokinetic studies using these mice were performed 8-12 weeks after transplantation of the human liver cells. Control NOG mice and humanized TK-NOG mice were administered 25 mg/kg clemizole PO, and blood samples were collected 30 minutes after dosing. The C57BL/6J mice (3 per time point) were dosed with 25 mg/kg PO Clemizole, and blood samples were collected at 15, 30 min and 1, 2, 4 and 6 hrs after dosing for analysis. For the drug-drug interaction studies, eight humanized TK-NOG mice were dosed with Clemizole (25 mg/kg P.O.) with or without ritonavir (20 mg/kg P.O), and blood samples were collected 30 minutes after dosing. Six of these mice were also treated with debrisoquine (10 mg/kg PO), in the presence or absence of ritonavir (20 mg/kg PO), and plasma obtained 2 hrs later for analysis.

Statistical analysis of mouse pharmacokinetic data. To assess the statistical significance of the difference in the relative amount of each metabolite (clemizole, M1, M2, M6, M12, M14 and M15) in plasma obtained from control and humanized TK-NOG mice, a two-sample two-sided t test was used. Of note, the amount of M1 was < 7 in all 8 of the control mice, while it was > 7 in all but one of the humanized TK-NOG mice. The two-sample two-sided t test result indicated that this difference in M1 abundance was highly significant (p value = 0.0004). In the DDI studies, a paired-sample t test was used to compare the amount of each of the metabolites (Figure 2) and for the clemizole AUC (0-12hr) (Figure 3) measured in the presence and absence of ritonavir co-administration. The paired-sample t test was also used to compare the relative amounts of 4-OH debrisoquine in the 6 humanized TK-NOG mice measured in the presence or absence of ritonavir co-administration.

Quantitative analysis of clemizole and metabolites in plasma. Mouse plasma (50 uL) was treated with acetonitrile with 0.1% formic acid (200 uL), vortexed and incubated at -20 ^{0}C for one

hour, centrifuged at 10,000 rpm for 10 min. The supernatants were collected, dried and resuspended in 50uL 5% acetonitrile with 0.1% formic acid for the analysis by LC/MS. HPLC was performed using an Agilent 1200 column compartment, capillary pump, and an autosampler on a Zorbax C18 column, 0.5x150 mm. The flow rate was 20 mL/min with a gradient from 5% solvent B (acetonitrile with 0.1% formic acid; solvent A is 0.1% formic acid in water) to 95% B in 30 min and held at 95% B for 5 min. Mass spectrometric analysis were carried out on an Agilent Model 6520 qTOF mass spectrometer equipped with an ESI source. The heated capillary temperature in the source was held at 325^{o}C. Full scan (m/z 110–1000) spectra or data dependent MS/MS spectra were collected. The metabolites were identified based on their collision-induced dissociation behavior in tandem mass spectrometry, accurate mass and retention time. Quantitative analysis of clemizole was performed using a calibration curve at 9-1257 ng/ml clemizole spiked into blank mouse plasma and extracted as above. An internal standard 1-(p-bromobenzyl)-2-(1-pyrrolidinylmethyl)- Benzimidazole was also spiked in at 1000ng/ml. Relative amounts of clemizole and metabolites in each sample were calculated using the assumption that all compounds had the same MS response factor.

Human pharmacokinetic and metabolite studies. Phase 1b studies (to be reported elsewhere) were conducted in genotypes 1 and 2 HCV patients under IRB-approved protocols to investigate the safety and tolerability, pharmacokinetics, and pharmacodynamics of clemizole HCl (see www.Clinicaltrials.gov and approval by the University of Ankara Medical School Ethics Committee; study sponsor Eiger BioPharmaceuticals, Inc.). De-identified aliquots of excess material, which were not needed for clinical monitoring, were kindly provided by Wenjin Yang (Eiger BioPharmaceuticals, Inc.) to us for PK and metabolite analysis. The samples obtained were from human subjects that were administered 100 mg Clemizole P.O., with or without 100 mg ritonavir P.O. administered one hour before the clemizole, and blood samples were obtained 0 to 12 hrs after dosing. The relative abundance of clemizole and its metabolites in plasma

were measured in samples obtained from 10 patients treated with clemizole alone, and from 3 patients who participated in the subcomponent evaluating the effect of ritonavir co-administration, by LC/MS analysis as described below.

Microsome incubations and analysis. Clemizole (20 uM, diluted from 10 mM stock in DMSO) was mixed with human, rat or mouse liver microsomal proteins (1 mg/ml) in 100 mM potassium phosphate buffer (pH 7.4) supplemented with 1 mM glutathione and 5 mM $MgCl_2$ in a total volume of 1 ml. After 5 min pre-incubation at 37°C, the reactions were initiated by addition of 2 mM NADPH, and then quenched by addition of 1 mL ice cold acetonitrile after 60 min. Negative control samples contained NADPH with test compound added with the acetonitrile quench. HPLC was performed using an Agilent 1200 column compartment, capillary pump, and autosampler on a Zorbax C18 column, 0.5x150 mm. The flow rate was 20 μL/min with a gradient from 5% solvent B (acetonitrile with 0.1% formic acid; solvent A is 0.1% formic acid in water) to 95% B in 30 min and held at 95% B for 5 min. Mass spectrometric analysis were carried out on an Agilent Model 6520 quantitative Time Of Flight mass spectrometer equipped with an ESI source. The heated capillary temperature in the source was held at 325°C. Full scan (m/z 110–1000) spectra or data dependent MS/MS spectra were collected. The metabolites were identified based on their collision-induced dissociation behavior in tandem mass spectrometry, accurate mass and retention time. Relative amounts of clemizole and metabolites in each sample were calculated using the assumption that all compounds had the same MS response factor.

Hepatocyte incubations. Using wide-bore pipette tips, aliquot 0.1 mL cell suspension into a 24 well plate, and the plates were incubated for at least 0.5 hr in a 37 °C incubator on shaker (500 rpm). Two wells of volume 0.5 mL were run for each test compound. Incubation mixtures (0.5 mL) contained test compound (20 uM with a maximum of 1% dimethyl sulfoxide used as

cosolvent) in Gibco HepatoZYME (Invitrogen, Carlsbad, CA, USA) media supplemented with 5% fetal bovine serum and 2mM L-glutamine and were allowed to react for 4 h. All incubations were quenched with an equal volume of acetonitrile, the duplicate wells combined, followed by centrifugation, evaporation to dryness and reconstitution in 10% acetonitrile in water. Negative control samples contained test compound only added with the acetonitrile quench. HPLC was performed using an Agilent (Santa Clara, CA, USA) 1100 column compartment, binary pump, autosampler and diode-array detector on a Varian (Palo Alto, CA, USA) Polaris 5 micron, C18-A column, 2.1x250 mm, in a column heater at 55^{o}C. The flow rate was 0.3 mL/min with a gradient from 0%(after a 5 min hold) solvent B (acetonitrile with 0.1% formic acid; solvent A is 0.1% formic acid in water) to 30% B in 25 min and held at 95% B for 5 min. Mass spectrometric analysis were carried out on a Thermo-Fisher (San Jose, CA, USA) LTQ Orbitrap mass spectrometer equipped with an ESI source. The heated capillary temperature in the source was held at 250^{o}C. Full scan positive spectra were collected along with MS/MS spectra for the major two peaks with the Orbitrap. Corresponding positive ion MS^3 spectra were collected with the LTQ low resolution detector. Negative full scan (m/z 180–900), MS/MS and MS^3 spectra were collected with the LTQ low resolution detector. Relative quantitative analyses were based on UV integration (276 nm) of identified peaks.

CYP reaction phenotyping. The reaction phenotyping was conducted using cDNAs expressing recombinant hCYP450 enzymes. (rhCYP 1A2, 2C8, 2C9, 2C19, 2D6, 3A4) and control preparations from baculovirus-infected Sf9 insect cells (supersomes) that were purchased from BD Gentest (Woburn, MA). Cytochrome c reductase was co-expressed in all preparations, and cytochrome b5 was expressed in cDNA-expressed CYP2C8, 2C9, 2C19, and 3A4. Incubation mixtures were prepared containing potassium phosphate buffer (50 mM, pH 7.4), magnesium chloride (5 mM), rhCYP450 enzymes (varied CYP concentration at pmole/ml with total 0.5 mg protein/ml), and clemizole (1 μM). The reaction mixtures were pre-incubated at 37°C for five

minutes prior to initiation of reactions with NADPH (2 mM final concentration) and stopped by addition of acetonitrile (1:1 by volume) at pre-determined time points (0, 5, 10, 20 min). Following quenching, one volume of sample was transferred to an injection plate containing one volume acetonitrile/water with internal standard. Samples were centrifuged at 3000 rpm for 10 min and the supernatants were collected for the analysis by LC/MS. Quantitative analysis of clemizole depletion was conducted using LC/MS/MS on an ABI 4000 mass spectrometer using MRM (mz 326 to m/z 255) with sample introduction on LC system containing a Shimadzu 20ADP binary pumps (Columbia, MD) and HTC PAL autosampler (Leap Technologies, Cary, NC), and a Hypersil C18 column(2.1x50 mm). The flow rate was 0.4 mL/min with a gradient from 5%(after a 1 min hold) solvent B (Acetonitrile: Methanol (50:50) with 0.1% Formic Acid) and 95% solvent A (5 mM Ammonium Acetate with 0.1% Formic Acid) to 90% B in 3 min and held at 90% B for 1 min. Formation of predicted metabolites (m/z 326 to m/z 255 for parent; 340 to 255 for M1;342 to 271 for M4; 324 to 255 for M2) were monitored on ABI 4000 QTrap mass spectrometer using the using multiple reaction monitoring triggered enhanced product ion scanning to obtain representative MS/MS spectra for the major metabolites (MRM-EPI). The LC method is similar as previously described, except for the column and run time. A Hypersil C18 column, 2.1x100mm, was used and total run time is 25 min.

Supplemental References

Chiu SH, Huskey SW (1998) Species differences in N-glucuronidation. Drug Metab Dispos 26:838-847.

Danielson PB (2002) The cytochrome P450 superfamily: biochemistry, evolution and drug metabolism in humans. Curr Drug Metab 3:561-597.

Fitch WL, He L, Tu YP, Alexandrova L (2007) Application of polarity switching in the identification of the metabolites of RO9237. Rapid Commun Mass Spectrom 21:1661-1668.

Hasegawa M, Kawai K, Mitsui T, Taniguchi K, Monnai M, Wakui M, Ito M, Suematsu M, Peltz G, Nakamura M, Suemizu H (2011) The reconstituted 'humanized Liver' in TK-NOG mice is mature and functional. Biochem Biophys Res Commun 405:405-410.

Proctor NJ, Tucker GT, Rostami-Hodjegan A (2004) Predicting drug clearance from recombinantly expressed CYPs: intersystem extrapolation factors. Xenobiotica 34:151-178.

Supplemental Table 1. LC/MS Characterization of clemizole and its metabolites. The retention times were measured using the hepatocyte LC method, and were adjusted for those few metabolites that were only detected *in vivo* or after incubation with microsomes.

Metabolite	Retention time	Nominal $[M+H]^+$	PPM error	Indicative MS/MS fragments	Indicative MS^3 fragments
Clemizole	14.0	326	2.8	255,125	220
M1	15.2	340	1.8	255,125	
M2	13.2	324	2.8	255,125	
M3	12.8	272	0.7	255,125	
M4	12.2	342	0.3	271,255	
M5	12.7	273	1.1	255,125	
M6	13.3	358	1.1	340,125	255
M7	14.0	356	2.2	338,255,125	
M8	11.7	289	2.4	271,259,125	
M9	12.5	356	0.6	271,125	
M10	13.9	342	1.2	256,257,125	
M11	11.2	288	1.7	271,125	
M12	12.5	243	1.6	125	
M13	10.8	502	2.4	326	255
M14	10.6	518	2.5	342	271,125
M15	11.3	532	2.4	356	271,125
M16	12.6	532	1.9	338	255,125
M17	11.8	449	2.6	273	255,125
M18	10.6	548	2.1	530	372,271
M19	10.4	332*	0.2	356	271,125

Supplemental Table 2. The amount of clemizole and metabolites present after 20 mM clemizole was incubated with human, rat or mouse liver microsomes for 1 hr; or after incubation with rat or human hepatocytes for 30 minutes. The number indicates the % of the total identified metabolites. None of these metabolites were detected in control incubations. ND indicates that a metabolite was not detected

	Microsomes			Hepatocytes	
	Human	**Rat**	**Mouse**	**Human**	**Rat**
Clem	40.1	3	24.1	15	ND
M1	35.5	3.5	2.5	39	ND
M2	1.8	3.5	4.8	0.1	ND
M3	4.6	6.1	5.7	0.2	ND
M4	5.4	4.8	3.4	4	ND
M5	4	6.8	2.5	0.5	ND
M6	2.3	2.7	1.8	18	ND
M7	1	5.3	0.7	4.7	ND
M8	0.3	17.9	9.8	ND	ND
M9	2.9	37.1	19.2	4	1.1
M10	1.3	ND	ND	ND	3.7
M11	0.2	9.3	25.5	ND	ND
M12	0.6	ND	ND	1.2	1.1
M13	ND	ND	ND	3	ND
M14	ND	ND	ND	10	5.4
M15	ND	ND	ND	0.3	43.6
M16	ND	ND	ND	ND	13.1
M17	ND	ND	ND	ND	10.2
M18	ND	ND	ND	ND	10.9
M19	ND	ND	ND	ND	10.9

Supplemental Table 3. The identified metabolites present after incubation of the indicated concentration of 10 uM clemizole with the indicated expressed recombinant human CYP450 for 20 min. The minor Phase 1 metabolites M5-M12 were not observed in the CYP450 phenotyping experiments.

CYP450:	**1a2**	**2b6**	**2c8**	**2c9**	**2c19**	**2d6**	**3a4**
Metabolites:	M2	M2	M2	M2	M2	M1	M1
	M4			M4		M2	M2

Supplemental Table 4. The age and sex of the 6 different human hepatocyte donors whose cells were used to produce 8 chimeric mice are shown, along with the human serum albumin level measured at the time when the pharmacokinetic experiments were performed. The percentage of the liver that is humanized, which was calculated based upon the measured albumin level as described in (Hasegawa et al., 2011), is also indicated.

Human	Donor		Hu Alb	Human
Mouse #	Age	Sex	(mg/ml)	Liver (%)
1	4	F	4.2	42
2	34	M	1.5	15
3	4	F	1.6	16
4	34	M	2.2	22
5	52	F	2.7	27
6	49	F	1.3	13
7	23	M	7.0	70
8	57	M	1.6	16

Supplemental Figure Legends

Supplemental Figure 1. The top graphs show the measured plasma clemizole concentration at the indicated times after a single oral 25 mg/kg dose of clemizole was administered to Balb/c or NOG mice (4 mice per group). The bottom graphs show the relative normalized abundance of clemizole and metabolites in plasma at the indicated time after dosing. As was observed in C57BL6 mice, clemizole was rapidly metabolized to 2 (M12 and M14) metabolites, while only minimal amounts of M1 or M6 were produced. The metabolite structures are shown in Figure 2.

Supplemental Figure 2. Reconstructed LC/MS chromatograms showing the relative amounts of clemizole and metabolites present after incubation of 20 uM clemizole with human, rat or mouse liver microsomes for 60 minutes. The peaks for clemizole (P), and the major human (M1) or rodent (M8, M9) metabolites are indicated.

Supplemental Figure 3. The % of clemizole remaining after 1 uM clemizole was incubated with control insect cells or with insect cells expressing the indicated recombinant CYP450 enzymes for 20 min.

Supplemental Figure 4. The relative amount of M1 produced after 20 uM clemizole was incubated with human liver microsomes in the presence of the indicated concentrations of ritonavir or omiprazole for 60 minutes.

Fig S1

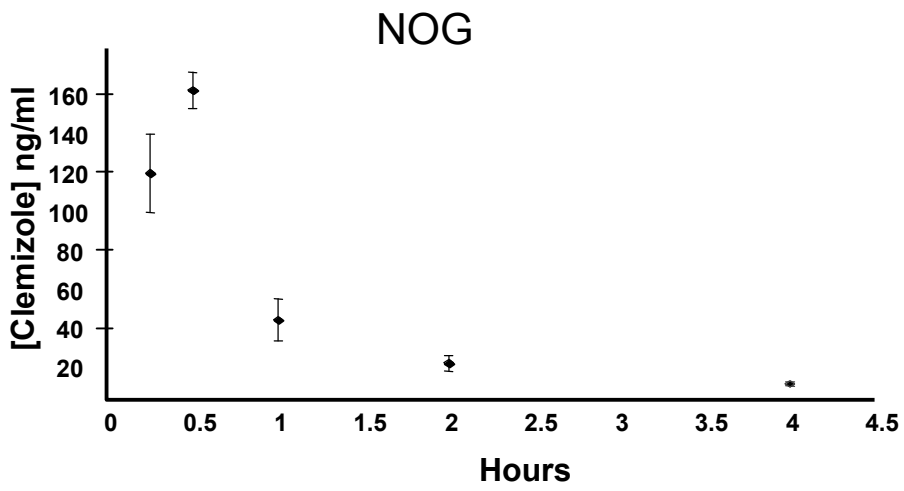
NOG
[Clemizole] ng/ml
160
140
120
100
80
60
40
20
0
0.5
1
1.5
2
2.5
3
3.5
4
4.5
Hours

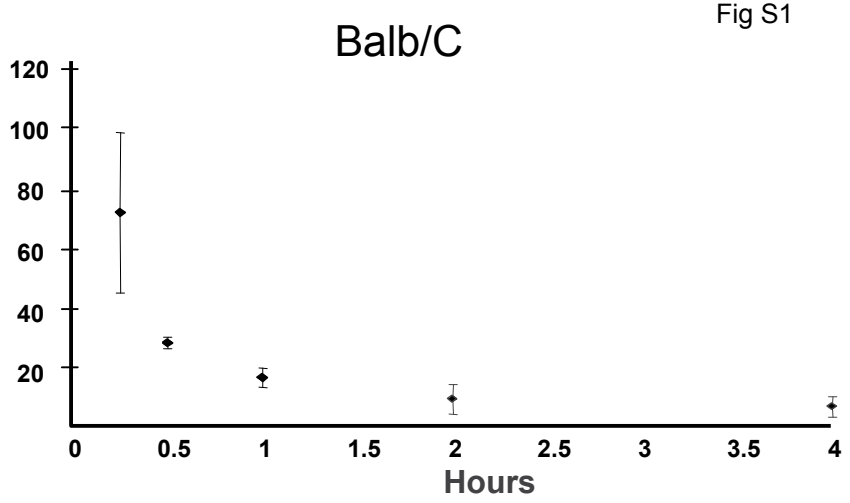
Balb/C
120
100
80
60
40
20
0
0.5
1
1.5
2
2.5
3
3.5
4
Hours

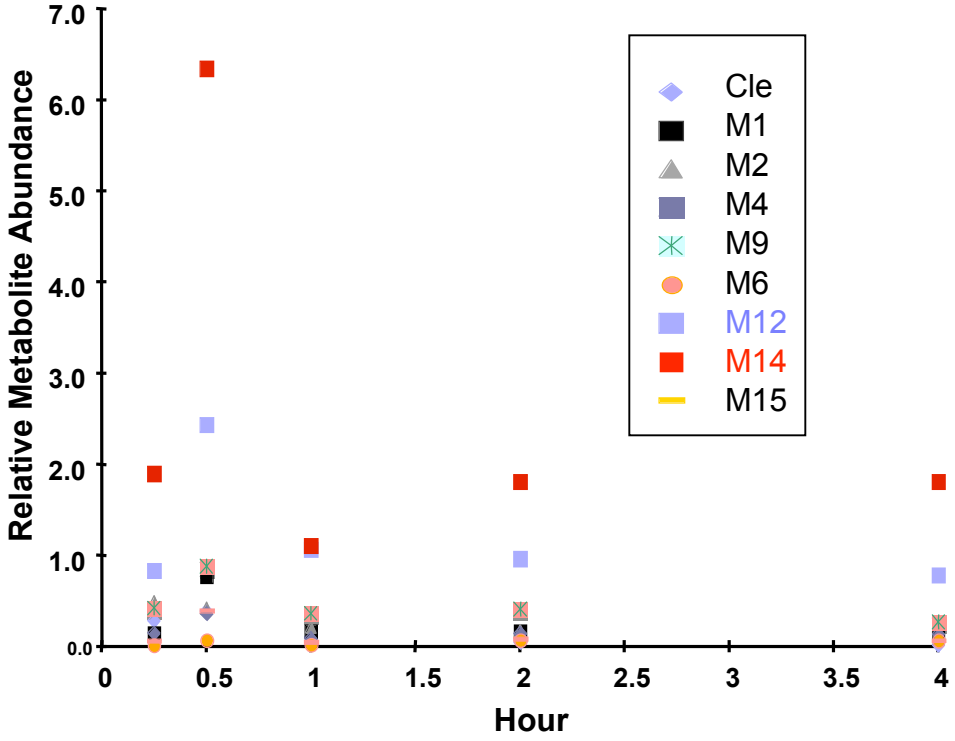
Relative Metabolite Abundance
7.0
6.0
5.0
4.0
3.0
2.0
1.0
0.0
0
0.5
1
1.5
2
2.5
3
3.5
4
Hour
Cle
M1
M2
M4
M9
M6
M12
M14
M15

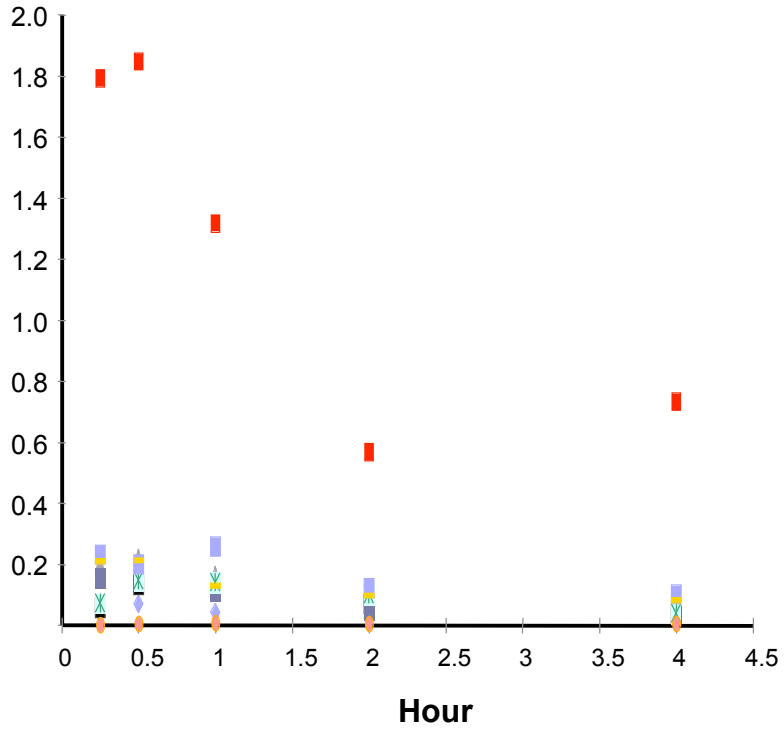
2.0
1.8
1.6
1.4
1.2
1.0
0.8
0.6
0.4
0.2
0
0.5
1
1.5
2
2.5
3
3.5
4
4.5
Hour

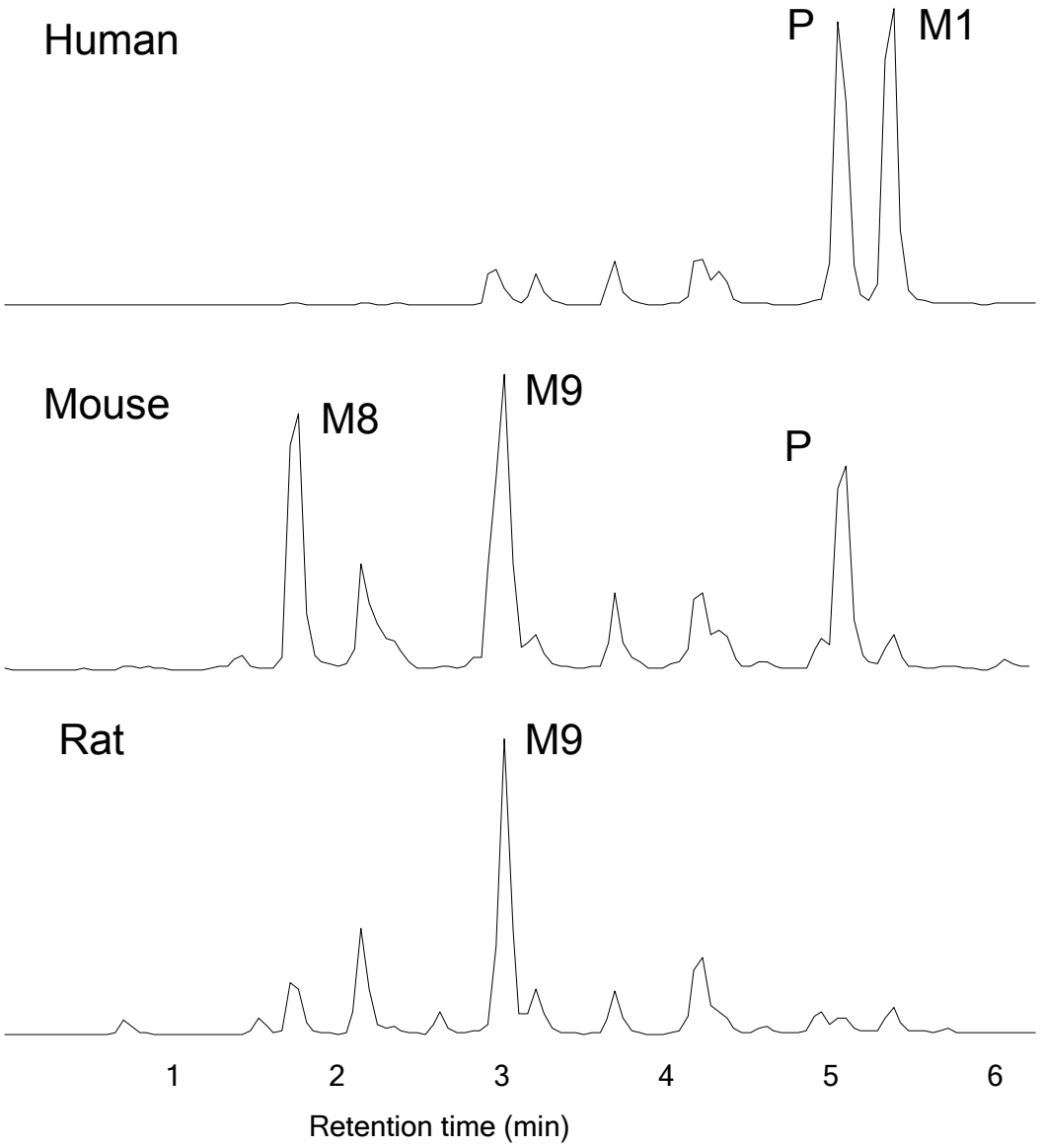
Human
P
M1
Mouse
M8
M9
P
Rat
M9
1
2
3
4
5
6
Retention time (min)

Fig S3

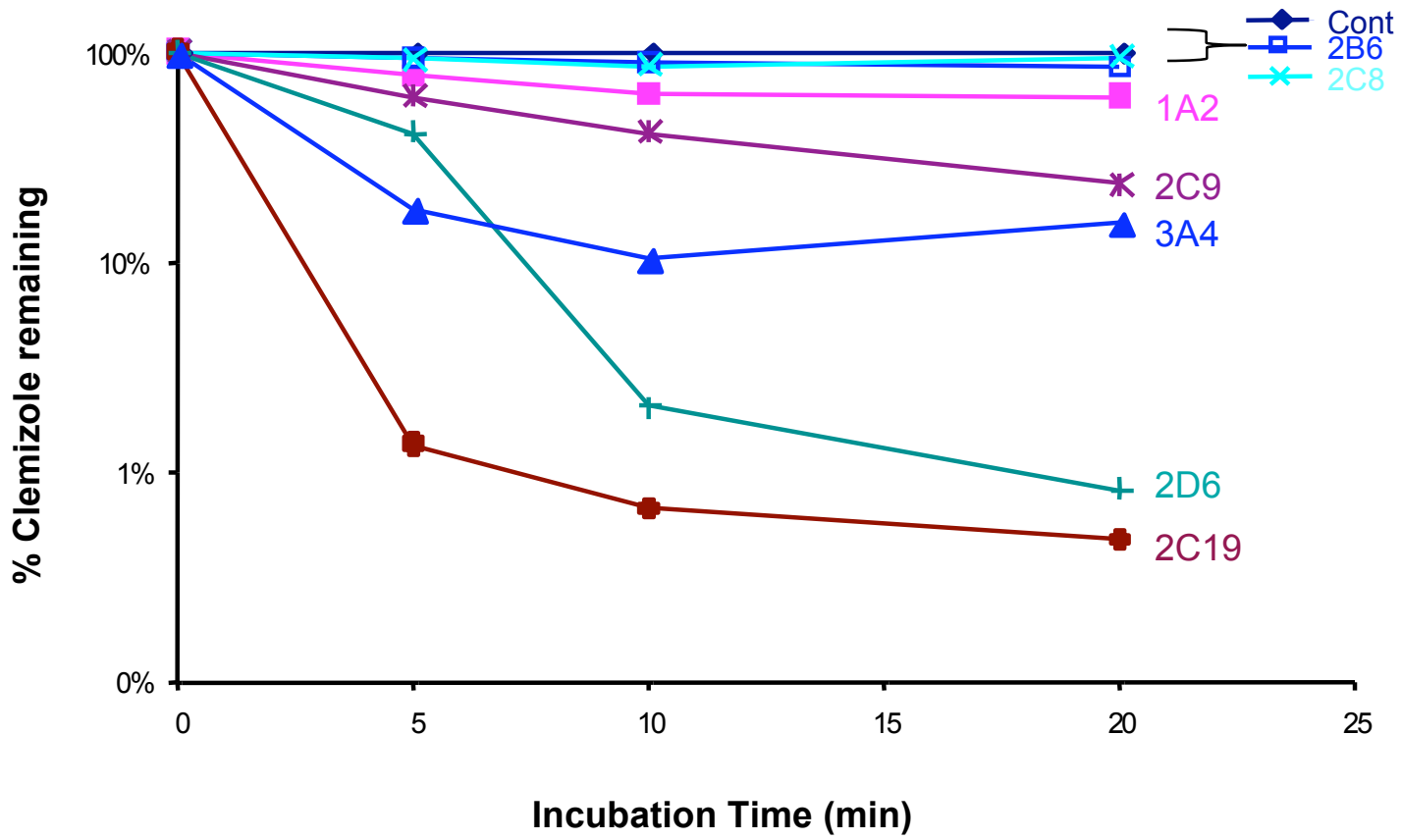
% Clemizole remaining
100%
10%
1%
0%
0
5
10
15
20
25
Incubation Time (min)
Cont
2B6
2C8
1A2
2C9
3A4
2D6
2C19

Fig S4

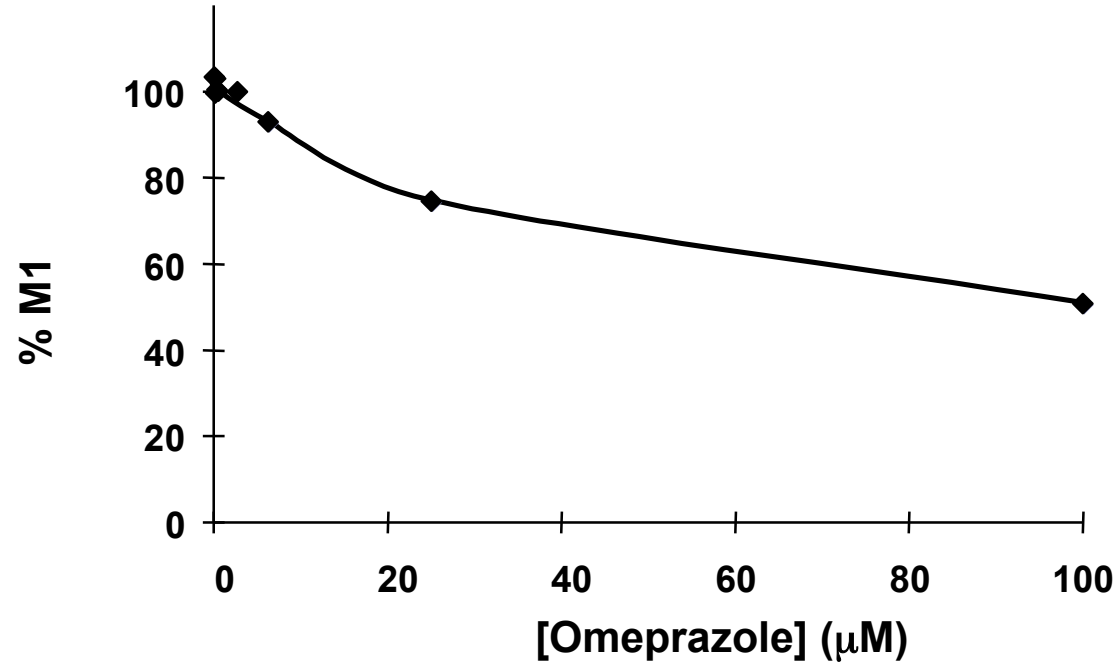
% M1
100
80
60
40
20
0
0
20
40
60
80
100
[Omeprazole] (μM)

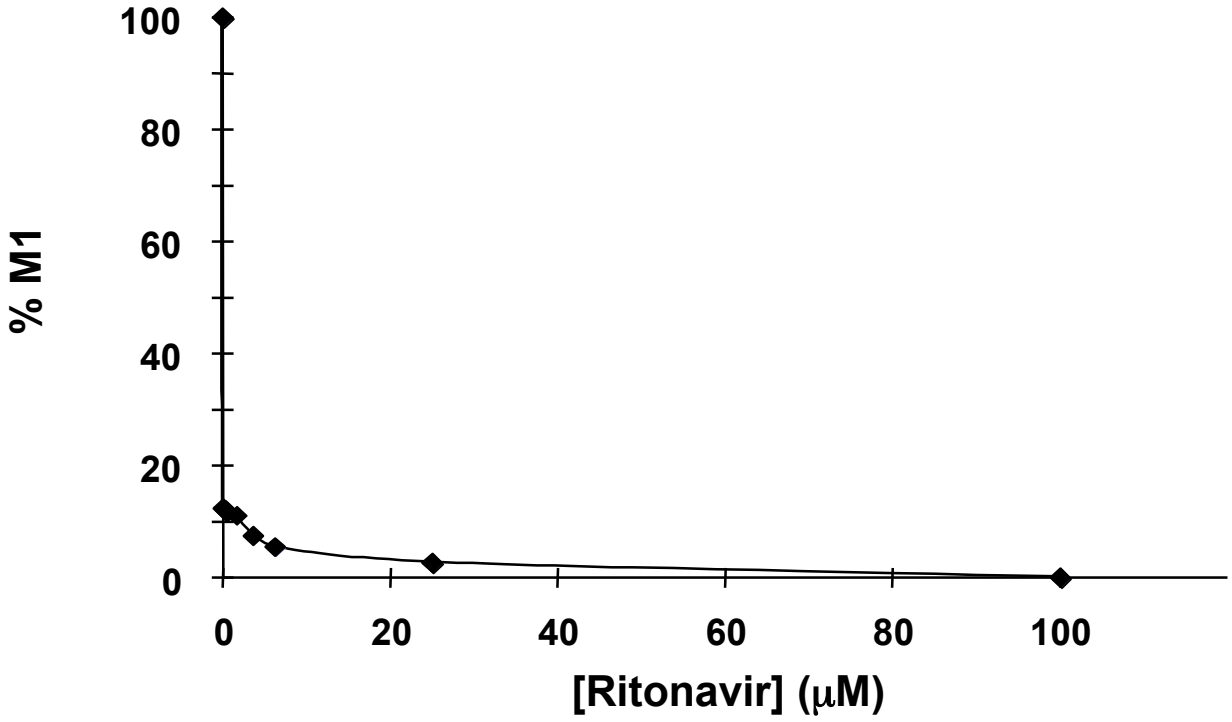
% M1
100
80
60
40
20
0
0
20
40
60
80
100
[Ritonavir] (μM)